004780-1-T

Mandel'shtam - Brillouin Scattering of CO_2 Laser Light from the Atmosphere as a Remote Sensing Probe

ANDERS DANIELS

January 1971

National Aeronautics and Space Administration
Grant No. NGR 23-005-452
Langley Research Center
Hampton, Virginia

High Altitude Engineering Laboratory
Departments of Aerospace Engineering
Meteorology and Oceanography

This report was also a dissertation submitted in partial fulfillment of the requirements for the degree of Doctor of Philosophy in the University of Michigan 1971.

THE UNIVERSITY OF MICHIGAN
COLLEGE OF ENGINEERING
High Altitude Engineering Laboratory
Departments of
Aerospace Engineering
Meteorology and Oceanography

Technical Report

MANDEL'SHTAM - BRILLOUIN SCATTERING OF CO_2 LASER LIGHT FROM THE ATMOSPHERE AS A REMOTE SENSING PROBE

ORA Project 004780

under contract with:
NATIONAL AERONAUTICS AND SPACE ADMINISTRATION
GRANT NO. NGR 23-005~~0~~452
Langley Research Center

administered through

OFFICE OF RESEARCH ADMINISTRATION ANN ARBOR

January 1971

TABLE OF CONTENTS

TABLE OF CONTENTS (continued)

LIST OF FIGURES

LIST OF FIGURES (Continued)

LIST OF FIGURES (Concluded)

LIST OF SYMBOLS

A	returned signal from the atmosphere
A_R	receiver aperture
A_r	cross-section of a scattering volume at altitude r
a	radius of an aerosol particle
C	returned signal with chopper obstructing the light from the atmosphere
c	speed of light and concentration of an atmospheric constituent
c_p	specific heat of air at constant pressure
c_v	specific heat of air at constant volume
D	difference in return signal between two successive chopper periods
dr	volume element at altitude r
δ	parameter in Equation 22
δ_c	parameter in Equation 36
δn	number of phonons in a frequency interval
$\vec{E}_o$	electric field vector of incident light
$\vec{E}_s$	electric field vector of scattered light
$\vec{E}_1'$	electric field vector of scattered light from volume element V_1
$\vec{E}_2'$	electric field vector of scattered light from volume element V_2
$\vec{E}''$	electric field vector of scattered light caused by density fluctuations
e	water vapor pressure
ε	dielectric constant
$\vec{E}$	electric field vector of scattered light modified by the time variations of density fluctuations
η	shear viscosity
η'	bulk viscosity
Δf	full width at half power of receiver response curve

LIST OF SYMBOLS (continued)

$\phi(t)$	time variation of density fluctuations
γ	ratio of specific heats
T'	parameter in Equation 19
γ_e	electrostrictive constant
$\hbar$	Planck's constant divided by 2π
I_o	intensity of incident light
I_s	intensity of scattered light
I_c	intensity of scattered light from concentration fluctuations
I_{MB}	intensity of scattered light into one M-B peak
I_{V^*}	intensity of scattered light from the volume element V^*
k	Boltzmann's constant
$\vec{K}_o$	wave vector of incident light
$\vec{K}_s$	wave vector of scattered light
α	coefficient of thermal conductivity
L	distance from scattering volume to observer
$\bar{l}$	molecular mean free path
λ_o	wave length of incident light
Λ	wave length of density fluctuations
N	number of molecules in a volume element
$N(r)$	number of molecules per unit volume at altitude r
N_L	Loschmidt number
n	index of refraction
ω_o	angular frequency of incident light
ω_s	angular frequency of scattered light
Ω'	parameter in Equation 22
Ω	angular frequency of density wave

ABSTRACT

The objective of this study is to verify spontaneous Mandel'shtam-Brillouin (M-B) scattering of 10μ CO_2 laser light in the atmosphere. Since the wavelength of this laser light is much longer than the mean free path of the molecules (STP), the radiation will no longer be scattered by individual molecules but rather by larger random density inhomogeneities. The corresponding pressure fluctuations move with the speed of sound and the return signal will therefore exhibit a net shift proportional to the sound velocity which in turn will be indicative of the temperature of the air. The return signal will furthermore exhibit a broadening inversely proportional to the density of the media. Thus by determining the spectral profile and frequency of the backscattered light one should be able to establish the temperature and density of the air without knowing the total return signal, which has been required in earlier remote atmospheric sensing investigations.

The theory for Mandel'shtam-Brillouin scattering is first reviewed and applied to the atmosphere. The feasibility of an experiment to observe spontaneous scattering is determined by calculating the expected signal to noise ratio of the returned radiation. This calculation shows that the return signal can be detected only by using time integration and a very stable laser system. To verify the theory a CO_2 laser system was constructed with power and temporal stability as design criteria. The scattered light was detected using homodyne detection. The signal from the detector was analyzed by a frequency selective receiver having a low frequency output, which was recorded and later integrated. A chopper provided the background signal for subsequent subtraction and normalization. Various recording, integrating and chopper arrangements

were used.

About thirty experimental runs were made in the frequency interval of 55 to 80 MHz where the returned signals were expected from theoretical calculations. An analysis of the data showed a signal increase for a frequency of 69-72 MHz and a halfwidth of 4-5 MHz, which correspond approximately to the predicted values. In addition a pronounced signal at 61 MHz with a halfwidth of 3-4 MHz is observed and behaves qualitatively as one would predict for stimulated emission. An analysis of the errors involved did not reveal instrumental or other effects that could have caused these features.

CHAPTER 1

SCATTERING OF LIGHT FOR AN OPTICAL WAVELENGTH GREATER THAN THE MOLECULAR MEAN FREE PATH

1.1 INTRODUCTION

Remote sensing of atmospheric parameters is truly one of the most pertinent problems in meteorology of today. With the advent of the laser several attempts were made to use this unique source of light for atmospheric sensing.

In the first experiments one determined the total intensity of laser light scattered back from the atmosphere and after subtraction of the Rayleigh scattering from a standard atmosphere the result was interpreted as an aerosol and water droplet density profile.[1] However it is also desirable to determine the molecular density by remote sensing methods, and a number of schemes to achieve this were developed. One scheme used a laser which could be made to change its radiating frequency from a spectral region where an atmospheric constituent absorbed radiation to another frequency where no absorption took place[2], or to a frequency corresponding to the Raman component of the scattered light[3]; the difference in signals could then be interpreted as representing a density profile of the constituent.

Another method, also suggested by Schotland,[4] is to determine the frequency spectrum of the returned radiation, since the difference in velocity between molecules and aerosols should separate the return signal when viewed in frequency space; Schotland further suggests that the temperature of the medium can be inferred from the frequency distribution of the light scattered by molecules. This distribution should

exhibit a broadening characteristic of molecules moving according to a Maxwellian velocity distribution. He concludes that the only type of laser that can be used is a gas laser (e.g. a CO_2 laser) since the relatively broad frequency spectrum of the solid state lasers would completely mask any change in the frequency of the returned light. However, if one uses a CO_2 laser with energy corresponding to a wavelength of 10.6μ, the individual molecules will not act as scatterers of the laser light since here the laser wavelength is two orders of magnitude larger than the mean free path of the molecules. In this case the scattering will no longer come from individual molecules, but from larger random density fluctuations in the medium. This theory of scattering [5] - known as Mandelstham Brillouin scattering (MB) - will be summarized and the results interpreted in terms of meteorological parameters. The feasibility, description, and results of the experiment which verify the theory are then presented.

1.2 INTENSITY OF SCATTERED LIGHT

Following Fabelinskii[5], consider a plane monochromatic light wave incident on a homogeneous medium of fixed molecules. These molecules will oscillate with the incident radiation and therefore emit secondary or scattered radiation with a definite amplitude and phase relative to each other. This situation is depicted in Figure 1 below, where a-a' is the wavefront and V_1^* and V_2^* are two volume elements with equal volume and with linear dimensions small compared with the wavelength of the incident radiation. Since the medium is homogeneous, the two volumes will contain the same number of molecules.

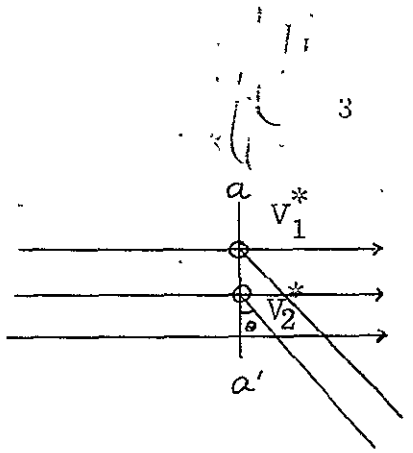

Figure 1. Scattering from stationary scattering volumes

At some direction θ it will always be possible to find a volume element V_2^* such that the scattered radiation from this volume will be of the same amplitude, but of opposite phase to the scattered radiation from another volume element V_1^* since all molecules radiate with definite phases and amplitudes to each other and are stationary. The two waves will therefore cancel each other in the direction θ and no net scattered intensity will be observed in this direction. The above discussion can, of course, be generalized to any direction, except forward and to any position of the wavefront. It can therefore be concluded that it is necessary to have inhomogeneities in a medium to get a net scattered intensity of incident radiation.

If we now let the previously fixed molecules execute random thermal motion but still retain the same number of molecules in each volume, the phases of the scattered radiation from the two previously defined volume elements are no longer related, and they will produce noncoherent radiation yielding a net scattering given by the addition of the square of the amplitudes of the incident light waves.

For the case where the mean free path of the molecules is much larger than the wavelength of the incident light, Rayleigh showed that the thermal motion of the molecules produces random phases of the

scattered light which result in noncoherent scattered radiation, the intensity of which is given by the well-known Rayleigh formula. This theory is briefly summarized below.

The absolute value of the flux vector of electromagnetic energy, S, and intensity, I, is related to the electric field by[5],

$$I = |\vec{S}| = \frac{cn|\vec{E}^2|}{4\pi} \tag{1}$$

where c is the speed of light and n is the index of refraction. For one molecule the electric field of the scattered light, $\vec{E}'_s$, the incident field $\vec{E}_0$ and the induced polarization $\vec{P}$ are related by[5],

$$\vec{E}'_s = \frac{\partial^2 P}{\partial t^2} \frac{\sin\theta}{L c^2}$$

$$P = \frac{(\varepsilon - 1)\ \vec{E}_0}{4\pi N_L} \tag{2}$$

where L is the distance from the observer to the scattering molecule, θ is the angle between the incident light field, $\vec{E}_0$, and the scattered light, N_L is Loschmidts number and ε the dielectric constant. The total scattered energy I, from a volume V, consisting of noncoherently radiating molecules, is given by adding the intensities from individual molecules yielding, with (1) and (2), the Rayleigh formula,

$$I = I_0 \frac{(\varepsilon - 1)^2 \pi^2}{\lambda_0^4 N_L L^2} \tag{3}$$

For the case where the mean free path of the molecules is much smaller than the wavelength of the incident radiation, the Rayleigh theory is no longer valid. Since the medium is approximately homogeneous, the thermal motions of individual molecules do not provide inhomogeneities on a scale large enough compared with the wavelength of the incident light to produce any significant amount of noncoherent scattered radiation.

However, considerable radiation is still observed from a medium with a mean molecular free path less than the wavelength of the incident radiation, and this scattering is explained by the Mandelśtham-Brillouin (hereafter designated as M-B) scattering theory.

For an explanation of M-B scattering let us return to the previous scattering situation (Figure 1). Let the number of molecules in one of the volumes N increase by ΔN, while the number in the other volume remains constant. In addition to the initial scattering from the two volumes (equal amplitudes but opposite phase), one of the volumes will now radiate an additional wave, $\vec{E}'$, caused by scattering from the additional molecules. The total electric field of the scattered radiation from the volumes is now $(\vec{E}_1+\vec{E}' + \vec{E}_2)$ where $\vec{E}_1$ and $\vec{E}_2$ are of equal amplitude but of opposite phase. The intensity of light scattered by the addition to the electric field, $\vec{E}'$, can be calculated by assuming that the density fluctuations, ΔN, will, under the influence of the incident light $\vec{E}=E_0 \cos wt$, yield an additional polarization, $\vec{P}'$, in the volume V_1^* given by,

$$\vec{P}' = \frac{\Delta \epsilon}{4\pi} V_1^* \; E_0 \cos wt \qquad (4)$$

where $\Delta\epsilon$ now is the additional polarization per unit volume. When we combine this expression with (1) and (2) we get for the scattered intensity from the volume V_1^*,

$$I_{V_1^*} = \frac{I_0 \pi^2 (V_1^*)^2 \overline{\Delta\epsilon^2}}{2 \lambda_0^4 L^2} \qquad (5)$$

where λ_0 is the wavelength of the incident light and I_0 its intensity. Far from the critical point of the gas the scattering from separate volumes can be regarded as independent[5] if their linear dimensions $V^{1/3}$, obey the following criteria,

$$\bar{\ell} \prec V^{1/3} \prec \lambda_o \tag{6}$$

where $\bar{\ell}$ is the mean free path in the medium. Under these conditions one can simply add the scattered intensities from each individual scattering volume, V^* and the total intensity of light scattered I_s, from the entire volume V becomes,

$$I_s = \frac{V}{V^*} I_{V^*} = \frac{I_o \pi^2 V^* V}{2 \lambda^4 L^2} \overline{\Delta\varepsilon^2} \tag{7}$$

where V^*/V is the number of approximately equally sized scattering volumes. For a gas at low pressure the dielectric constant is related to the number of molecules in a scattering volume by,

$$(\varepsilon - 1) = C N_L = CN/V^* \tag{8}$$

and thus

$$\overline{\Delta \varepsilon}^2 = \frac{(\varepsilon-1)^2 \overline{\Delta N^2}}{N_L^2 (V^*)^2} \tag{9}$$

where C is some constant. With these last two expressions, the scattered intensity from the entire volume becomes,

$$I_s = \frac{I_o \pi^2 V (\varepsilon-1)^2}{2 L^2 \lambda_o^4 N_L} \tag{10}$$

As can be seen, this expression is identical to the one predicting Rayleigh scattering for the case where the mean free path of the molecules is much less than the wavelength of the incident light.

1.3 NATURE OF DENSITY INHOMOGENEITIES IN AIR

In the previous section we merely assumed the existence of density inhomogeneities. In this section we will discuss the origin and subsequent behavior of such density inhomogeneities for air far away from the critical point.

From a statistical viewpoint, it can be realized that the probability of having a uniform density in a gaseous medium is extremely small, i.e., there will always be differences in the density caused by the always present thermal motion of the molecules. Since these density fluctuations are nonequilibrium perturbations they are unstable and will instantaneously start to dissipate and give rise to new density fluctuations. In a viscous medium such as air the dissipation process will follow two processes, a mechanical one involving a net motion of molecules but no change in the thermal energy of the individual molecules and a thermal one resulting in a change in the thermal energy of the molecules but no net transport of molecules[7]. The mechanical process will thus create isothermal pressure waves or phonons which propagate in all directions of the medium. The phase velocity of these random pressure waves can be predicted by arguments identical to those used to determine the phase velocity of ordinary or driven sound waves and their speed of propagation will therefore be the same as that for ordinary "driven" sound waves. The random sound waves will manifest themselves as a continuous "noise" sound if one were to expose a very sensitive microphone to the medium. The number of such isothermal pressure waves or phonons, dZ, within a certain frequency range Ω to $\Omega + \delta\Omega$ in a volume V was first given by Debye[8]. His expression was developed for thermal waves in a solid, but can be extended to our situation,

$$dZ(\Omega) = \frac{3\,\Omega^2 V}{2\pi v^2}\, d\Omega \qquad (11)$$

where v is the phase velocity for the pressure waves in the medium. The minimum wavelength of these fluctuations can be shown[5] to be

$$\Lambda = \left(\frac{4\pi}{3}\right)^{1/3} \bar{\ell} \qquad (12)$$

where $\bar{\ell}$ is the mean free path of the molecules in the medium. For air at standard temperature and pressure $\Lambda \sim 0.5\,\mu$. At the larger wavelengths these density fluctuations probably proceed into the turbulence region. The second process to relieve the density perturbations, the isobaric thermal wave, will be stationary and decay in time by transferring the excess energy to the surrounding medium as a damped wave.

1.4 SCATTERING FROM MOVING ISOTHERMAL PRESSURE FLUCTUATIONS

To determine the effect of the motion of the scattering inhomogeneities consider Figure 2 below where $\vec{k}_o$ is the wave vector of the incident light, $\vec{k}_s$ that for the scattered light and $\vec{q}$ that for the travelling isothermal pressure wave.

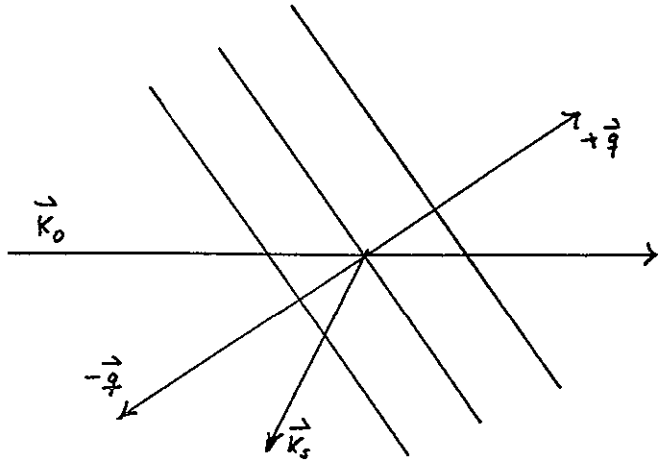

Figure 2. Scattering from a moving inhomogeneity

Conservation of energy in this situation requires that

$$\hbar \omega_s = \hbar \omega_o \pm \hbar \Omega \tag{13}$$

where $\hbar$ is the Planck constant divided by 2π and ω_s, ω_o are the angular frequencies for the light waves and Ω that for the pressure wave. A positive sign preceding $\vec{q}$ implies the creation of a photon, a negative sign the annihilation of one. It will, throughout this section, where we treat spontaneous scattering, be assumed that this addition or subtraction of energy from the density field does not significantly effect the density wave picture. Conservation of momentum, furthermore, requires

$$\vec{k}_s = \vec{k}_o \pm \vec{q} \tag{14}$$

The magnitudes of these vectors for the light waves can be expressed as

$$k_s = \frac{\omega_s n_s}{c} \quad \text{and} \quad k_o = \frac{\omega_o n_o}{c}$$

while that for the density wave will be $\vec{q} = \frac{\Omega}{v}$ where v is the phase velocity of the phonons and n_s and n_o are the indices of the refraction. This discussion is also valid for other types of inelastic scattering such as Raman and Compton scattering while for elastic scattering processes such as Rayleigh and Thompson scattering, $\Omega = 0$. The absolute value of Ω can be determined from Figure 3 below.

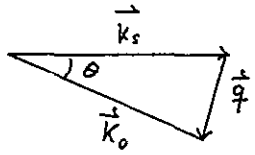

Figure 3. Scattering geometry for inelastic scattering.

It can be assumed that the indices of refraction for the incident wave, n_o, and that for the scattered light, n_s, are the same, n, and we can see from Figure 3 that

$$q = (k_o^2 + k_s^2 - 2 k_o k_s \cos \theta)^{1/2}$$

For $|k_0| \sim |k_s|$ this expression becomes

$$q = 2 k_0 \sin(\theta/2) \quad \text{and} \quad \Omega = 2 v n \frac{\omega_o}{c} \sin(\theta/2) \qquad (15)$$

The relative frequency change is given by

$$\frac{(\omega_s - \omega_o)}{\omega_o} = \frac{\Delta\omega_{MB}}{\omega_o} = \pm \frac{\Omega}{\omega_o} = 2n\frac{v}{c} \sin \theta/2 \qquad (16)$$

which thus predicts that scattering will occur at two frequencies, one shifted up in frequency corresponding to a phonon annihilation and one shifted down with the same frequency corresponding to a phonon creation. This net shift, $\Delta\omega_{MB}$, will be;

$$\Delta\omega_{MB} = 2 n v \frac{\omega_o}{c} \sin(\theta/2) \qquad (17)$$

So far we have assumed that these isothermal pressure waves do not dampen out as they travel through the medium. This will in reality not be the case since a viscous damping results in a broadening of the returned light. This broadening can be determined from Stokes law for the propagation of sound in a viscous medium[5]. We assume that the pressure fluctuations give rise to corresponding fluctuations in the index of refraction and that the pressure fluctuations can be described by a wave i.e. $\Delta n \sim \Delta p \sim \phi(t)$. where $\phi(t)$ represents the time variation of this fluctuation.

With these assumptions Stokes law gives

$$\frac{\partial^2 \phi}{\partial t^2} - v^2 \nabla^2 \phi - \Gamma \nabla^2 \left(\frac{\partial \phi}{\partial t}\right) = 0 \qquad (18)$$

where v is, as before, the phase velocity of the pressure wave and Γ is a measure of the damping given by

$$\Gamma = \frac{1}{\rho} \left\{ \frac{4}{3} \eta + \eta' + \frac{\kappa}{c_p} (\gamma - 1) \right\} \qquad (19)$$

where ρ is the density, η the shear viscosity, η' the bulk viscosity, κ the thermal conductivity and $\gamma = c_p / c_v$. We will seek a solution to this equation in the form of

$$\phi(t) = \phi_o e^{i (m t - \vec{q} \cdot \vec{r})} \qquad (20)$$

where $\vec{q}$ is the wave vector of the pressure wave and r is the radius vector from the observer to any scattering element inside the scattering volume. When we substitute (20) into (18) we get for m,

$$m = \frac{i \Gamma q^2}{2} \pm \left(q^2 v^2 - \frac{\Gamma^2 q^4}{4}\right)^{1/2} \qquad (21)$$

With this expression for m, the equation for a pressure wave may be written,

$$\phi(t) = \phi_o e^{-\delta t} \cos\left(\Omega' t - \vec{q} \cdot \vec{r}\right) \qquad (22)$$

where

$$\delta = \frac{\Gamma q^2}{2}$$

$$\Omega = v q$$

and

$$\Omega' = \pm (\Omega^2 - \delta^2)^{1/2} \qquad (23)$$

The electric vector of the original scattered light wave $\vec{E}'$, is modulated by the density wave to produce a new expression for the electric field of the scattered radiation $\vec{E}(t)$,

$$\vec{E}_s(t) = \vec{E}'(t)\,\phi(t) = \frac{\phi_o e^{-\delta t}}{2} E' e^{i\left[(\omega_o \pm \Omega')t - \vec{q}\cdot\vec{r}\right]} \tag{24}$$

The time variation in the intensity of this radiation I (t) is therefore[5]

$$I(t) = I_o\, e^{-2\delta g}\left\{1 + \cos^2\left[\Omega' t - \vec{q}\cdot\vec{r}\right]\right\}. \tag{25}$$

A Fourier transform into frequency space yields for the electric field,

$$E(t) = \int_{-\infty}^{\infty} E(\omega')\, e^{i\omega' t}\, d\omega' \tag{26}$$

where Fourier coefficients are given by,

$$E(\omega') = \frac{1}{\pi} \int_{o}^{\infty} E(t)\, e^{-i\omega' t}\, dt \tag{27}$$

Completing the integration in (27) we get for the intensity of light scattered from dampened pressure waves,

$$I(\omega') = \overline{\vec{E}(\omega')\cdot\vec{E}^{*}(\omega')} = \frac{\text{const}}{(\omega^2 - \Omega'^2)^2 + 4\delta^2\omega^2} \tag{28}$$

where $\omega = \omega' - \omega_o$ is a measure of the shift in frequency from the frequency of the incident light ω_o. If we denote the total scattered intensity from pressure fluctuations by $2\,I_{MB}$ we get

$$I(\omega_o \pm \omega) = \frac{\Omega_o^2\, \frac{2\delta}{\pi}\, 2\, I_{MB}}{(\omega^2 - \Omega'^2)^2 + 4\delta^2\omega^2} \tag{29}$$

where $2\,I_{MB} = \int_{-\infty}^{\infty} I(\omega)\, d\omega$

The location of the maximum of these scattering peaks - the MB satellites-is determined by,

$$\omega_{max} = \sqrt{\Omega'^2 - \delta^2} \tag{30}$$

and the full width at half power $\delta\omega_{MB}$ is,

$$\delta\omega_{MB} = 2\delta\left(1+\frac{1}{2}\frac{\delta}{\Omega'}\right) \approx 2\delta = \tau_q^{-2} = \tau'\frac{q^2\pi^2}{\lambda_o^2}\sin^2(\theta/2) \tag{31}$$

1.5 SPECTRAL DISTRIBUTION OF SCATTERING FROM STATIC ISOBARIC DENSITY FLUCTUATIONS

As stated in section 1.3 there will be in addition to moving isothermal pressure fluctuations stationary isobaric temperature fluctuations which also will give rise to scattered radiation. Since these fluctuations do not move there will be no net shift of the scattered radiation. These waves are also dampened in time and this again produces a broadening of the scattered radiation. To determine this broadening we proceed in a fashion analogous to that in the preceding section; we assume that the temperature fluctuations ΔT give rise to corresponding fluctuations in the index of refraction Δn and that the fluctuation is in the form of a wave $\phi(t)$, i. e.,

$$\Delta n \sim \Delta T \sim \phi(t) \tag{32}$$

The appropriate equation to use here is the equation of thermal conductivity,

$$\frac{\partial\phi}{\partial t} - \chi\nabla^2\phi = 0 \tag{33}$$

where χ is the coefficient of thermal conductivity. Again we write the desired solution as,

$$\phi(t) = \phi_o e^{-i(mt - \vec{q}\cdot\vec{r})} \tag{34}$$

and after substituting this equation into (33) we get,

$$\phi(t) = \phi_o e^{-\delta_c t} \quad e^{-i\vec{q}\cdot\vec{r}} \tag{35}$$

where δ_c is given by.

$$\delta_c = \chi q^2 \tag{36}$$

By analogy with the discussion in the previous section the intensity of these fluctuations can be shown to be,

$$I(\omega) = \frac{\frac{\delta_c}{\pi} I_c}{\omega^2 + \delta_c^2} \tag{37}$$

where I_c is the total intensity of the light scattered by the thermal waves. The full width at half intensity $\delta\omega_c$ is given by,

$$\delta\omega_c = \delta_c = \chi q^2 \tag{38}$$

It was shown earlier that the total scattered intensity from the two types of density fluctuations is identical to that from Rayleigh scattering. Landau and Plazek[9] furthermore showed that the ratio between the two components was given by,

$$\frac{I_c}{2 I_{MB}} = \frac{c_p - c_v}{c_v} = \gamma - 1 \tag{39}$$

1.6 SCATTERING FROM FLUCTUATIONS IN THE CONCENTRATION, AND AN ISOTROPIES OF MOLECULES

In the previous discussion it was implicitly assumed that there was only one species of molecules present. This is not the case for the atmosphere and the scattering picture is not complete without a

discussion of the effects on the scattering caused by variations in the concentrations of the constituents. These variations give rise to a fluctuation of the dielectric constant

$$\Delta \varepsilon_{conc} = \sum_i \left(\frac{\partial \varepsilon}{\partial c_i} \right) \Delta c_i \qquad (40)$$

where c_i is the concentration of the ith constituent. For the two main constituents in air, oxygen and nitrogen, the dielectric constants are nearly the same, 1.000523 and 1.000580 respectively. Since the actual variations in the concentrations are very small, fluctuations in the concentrations in the air will contribute insignificantly to the total scattering picture.

The anisotropy fluctuations of air molecules leads to a correction factor of $(6+3\rho_n)/(6-7\rho_n)$ in the scattered intensity (10) where ρ_n is the depolarization factor. For air, Penndorf[10] uses a value of 0.035 for ρ_n which yields a correction factor of 1.061, which gives a negligible correction to the intensity of the scattered light.

1.7 PHASE VELOCITY OF HIGH FREQUENCY SOUND

In the previous section, v has denoted the phase velocity of ordinary sound, i.e. of audible frequency. The frequency of the random sound waves we intend to measure in this work is much higher - about 70 MHz using a CO_2 laser as the light source. Ultrasound with a frequency up to 11 MHz[11] can be measured by transducer techniques while for higher frequencies sound velocity has only been investigated from the return of lasers and calculated according to the M-B scattering theory.

The only experiment reported, to the author's knowledge, which measured spontaneous M-B scattering in N_2 is that of Greytak and Benedek[12] (STP). Using a He-Ne laser they determined a 100 MHz sound velocity of 344 ± 7 m/s. Extrapolation of results from ultrasonic experiments (at 11 MHz) by conventional transducer techniques yields a 100 MHz sound velocity of 361 m/s for conditions identical to those during Greytak and Benedek's experiments.[11] It does not appear that the explanation for this discrepancy has been found yet.[13]

1.8 STIMULATED M-B SCATTERING

As shown earlier spontaneous M-B scattering involved an energy exchange between the radiation field and the phonon field. It was assumed that the effect of this exchange on the phonon field was negligible. Before the advent of the laser this was certainly a valid assumption. However with the use of a laser as the source for the scattering light this is no longer necessarily true and it has been demonstrated that the high incident energy densities from pulsed lasers can indeed alter the phonon field significantly.[14] This change in the phonon field is reflected in the scattered light. The theory for the scattering scheme that will apply to this situation - stimulated M-B scattering - is described below, and is primarily from Goldblatt.[14]

When a light wave is incident on a medium the electromagnetic field of the radiation creates a pressure wave through electrostriction. This electrostrictive pressure, P_{el}, is related to the energy flux of the light by the expression

$$P_{el} = (\gamma_e/8\pi)\ E_o^2 \tag{41}$$

where γ_e is the electrostatic constant given by $\gamma_e = \rho\frac{\partial \mathcal{E}}{\partial \rho}$ and ρ is the density. There will always be at least two electric fields present

in the medium - that from the incident radiation, E_0, and that from the scattered radiation, E_s. Where these two fields are colinear the electrostrictive pressure produced by the product of these two fields is;

$$P_{el}=(\sigma/8\pi)\left|(\vec{E}_0+\vec{E}_s)\right|^2=(\gamma_e/8\pi)E_0E_s e^{i(\vec{k}_o-\vec{k}_s)\cdot r-(\omega_o-\omega_s)t} + \text{terms of higher frequency} \qquad (42)$$

Thus the beat wave between the incident and the scattered light will produce a pressure wave of the same frequency as the originally scattering pressure wave. If the incident light isvery strong this pressure wave will be able to survive absorption and will in turn scatter more of the incident radiation resulting in an amplification of the induced pressure wave. This process can theoretically continue until the scattered light is equal to the incident light i. e. the intense laser light has by itself created a dielectric mirror colinear to the radiation.

There are initially two M-B scattering peaks from spontaneous scattering, one upshifted in frequency from sound waves moving toward the source (phonon annihilation) and one downshifted from sound waves moving away from the source (phonon creation). However only the downshifted peak will be amplified because the phonons must come from the weak random pressure fluctuations in the gas. Hence the source will quickly be exhausted. The created phonons, on the other hand, are arrived at by splitting the incident phonons which are 10^{18} times more numerous [14] than the thermal phonons. It should be remembered that this process will only take place if the created phonon is strong enough to sufficiently

overcome acoustic damping.

One might expect from the theory that this scattered radiation should be of the same frequency and exhibit the same broadening as the spontaneously scattered light. This has been shown not to be the case; in the few experiments carried out to establish high frequency velocity using stimulated M-B scattering for N_2, the results are shown in Table 1.

	Hagenlocker & Rado[15]	Mash et al[16]	Rank et al[17]	Saito[13]
$V_{(exptl)}$	330± 20	280 ±10	380+10	380
$V_{(theoret)}$	333	352	>380	>380

Table 1. Theoretical and experimentally found velocities for high frequency sound in m/s at 125 atm and 27° C using stimulated M-B scattering technique.

No measurements have been reported for the speed of high frequency sound at atmospheric pressures for air using stimulated M-B scattering but from the above values it can be concluded that at atmospheric pressures one can expect the speed of high frequency sound, as measured by stimulated M-B scattering, to be less than that expected when measured with other techniques e.g. spontaneous M-B scattering. There is a great increase in the absorption of the created sound wave and though this cannot explain the above mentioned discrepancies in the observed sound velocity[13], one can expect that the stimulated M-B component will be much narrower than the spontaneous M-B scattering. (see, e.g. equation (28) and (19)).

1.9 SUMMARY OF M-B SCATTERING AND ITS APPLICATION TO ATMOSPHERIC SENSING

Spontaneous M-B scattering, as shown in the sections 1.4 and 1.5, results in three peaks in the scattered return, a center peak formed

from light scattered by thermal fluctuations, and unshifted but broadened by the thermal conductivity of the medium, and two symmetrical peaks, one shifted up in frequency corresponding to phonon annihilation and one shifted down caused by the creation of phonons. These two shifted peaks will also be broadened, but by the viscosity of the medium rather than the thermal conductivity. The total intensity of the peaks is identical to that predicted by Rayleigh scattering theory although the physical processes are quite different. The intensity of the center peak is greater than that of the shifted peaks.

The net shift of the side peaks caused by spontaneous M-B scattering is proportional to the velocity of sound. It seems reasonable to assume that also for sound in the ultrasonic range there should be parameters similar to that for normal sound velocity given by[18]

$$v = 20.05\,(T^{1/2} + 0.14\,\frac{e}{p}) + W \quad (M/S) \qquad (43)$$

where T is the absolute temperature, e, the water vapour pressure, p, the atmospheric pressure, and W, the wind speed. If the wind component is neglected the sound velocity is approximately proportional to $T^{1/2}$ since the humidity effect is only of secondary importance. Thus one can write,

$$\Delta\omega_{MB} \propto \sqrt{T} \qquad (44)$$

The broadening of the M-B satellites is indirectly proportional to the density, while the quantities inside the bracket of the expression for $\delta\omega_{MB}$ (.(17) and (31))- the viscosity and the thermal conductivity - are independent of density but proportional to $T^{3/4}$. One can therefore write,[19]

$$\delta\omega_{MB} \propto T/\rho \tag{45}$$

Thus if temperature is determined from a measurement of $\Delta\omega_{MB}$ the expression for $\delta\omega_{MB}$ could be used to determine the density. The broadening of light scattered by isobaric density fluctuations is proportional to $\delta\omega_{MB}$ and this quantity would therefore not furnish any further information about the medium. If it were necessary to correct for the wind velocity in (43), a measurement of the frequency of the scattering from aerosols would yield this information.

Stimulated M-B scattering, which will occur only if the intensity of the incident radiation is sufficiently high, exhibits a behavior that is less predictable theoretically, but it should consist of only one peak shifted down in frequency by phonon creation. Experimentally it has been found that the speed of high frequency sound as determined by stimulated M-B scattering is less than that determined by other methods. The broadening is also less, caused by an increase in acoustic loss of the created sound waves. The peak in the return caused by stimulated M-B scattering is difficult to use in determining high frequency sound velocities and the related atmospheric parameters since the experimental values for high frequency sound show less agreement with theory than the corresponding spontaneous M-B scattering. This may indicate that the relations for the shift and width of the peak are not as simple as predicted[13]. It seems reasonable, however, to assume that there is a relation between the shape and net shift of the stimulated M-B peak and meteorological parameters. This relation would probably have to be determined experimentally.

Stimulated M-B scattering has the potential of becoming a powerful remote sensing tool since the very large returns would make experiments much easier. Spatial resolution could be achieved by combining the advantages of a CW laser system with those of an identical transmitter-receiver system. This could be done by focusing the light on the altitude one wants to probe.

CHAPTER 2

APPLICATION OF THE SCATTERING THEORY TO 10.6μ CO_2 LASER LIGHT SCATTERED FROM THE ATMOSPHERE

2.1 PREDICTED FREQUENCY DISTRIBUTION OF SCATTERED LIGHT NEAR THE SURFACE ($\bar{\ell} \sim 10^{-5}$ cm)

When the atmosphere is irradiated by CO_2 laser light ($\lambda/n \sim 10^{-3}$cm), the requirements for the scattering theory previously discussed are fulfilled i.e. $\lambda/n \gg \bar{\ell}$. Typical numerical values for the parameters involved in the expressions for $\Delta\omega_{MB}$, $d\omega_{MB}$, $d\omega_c$ are listed below.

$v = 3.6 \times 10^{+4}$ cm/sec

$n = 1.0003$

$\rho = 1.3 \times 10^{-3}$ gr/cm^3

$\eta = 1.7 \times 10^{-4}$ gr/cm^3

$\eta' = 0$ (small enough to be neglected)

$\kappa = 2.4 \times 10^{3}$ erg/sec, cm, C^o

$c_p = 10^7$ cm^2/sec, C^o

$\gamma = 10/7$

$\Gamma = 0.25$ cm^2/sec

$\chi = 0.20$ cm^2/sec

$\lambda/n = 1.06 \times 10^{-3}$ cm

With these values inserted into (17) (31) and (38) we get the following values,

$\Delta\omega_{MB} = 68$ MHz

$d\omega_{MB} = 2\pi$ MHz

$d\omega_c = 1.6\pi$ MHz

Figure 4 thus depicts the frequency distribution of CO_2 laser light scattered back from the atmosphere.

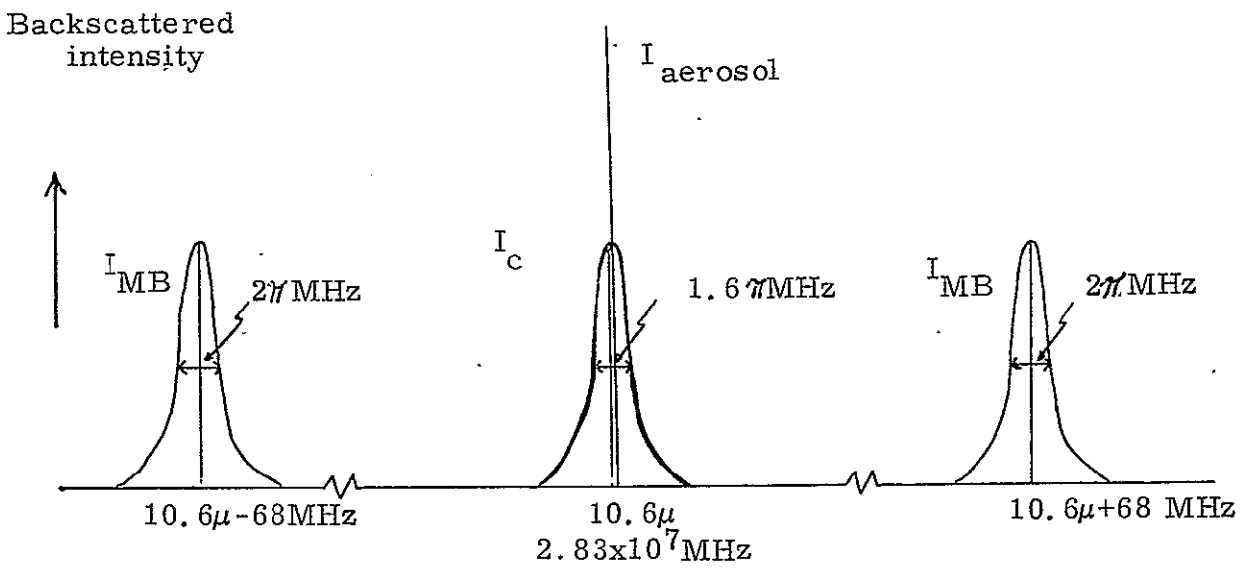

Figure 4. Expected frequency distribution of CO_2 laser light scattered from the atmosphere

The integrated intensities of the above three peaks are about equal.[9] In the next section we will arrive at an expression for the expected signal to noise ratio for scattering into the MB peaks. There will be a relatively large component in the total return scattered by aerosols. Since these move with the wind velocity the incident frequency will be shifted according to Doppler's theory by an amount $\Delta\omega_{aerosol}$ equal to,

$$\Delta\omega_{aerosol} = \frac{4\pi nW}{\lambda_o} \qquad (46)$$

where n is the index of refraction and W is wind velocity, which for vertical velocities of the order of cm/sec will be about a few KHz. This return will also be broadened with a halfwidth $d\omega_{aerosol}$ of[2],

$$d\omega_{aerosol} = \frac{2kT}{3\eta\lambda_o^2 a} \qquad (47)$$

With a particle radius, a, of about 1 micron or larger this broadening will be of the order of KHz or less and will therefore not interfere with the other scattering distributions except in a narrow interval near the frequency of the incident light.

It has been assumed that the incident light is monochromatic, plane polarized and has a plane wavefront. However, no light sources, including lasers, are truly monochromatic, but in comparison with the spectrum of the molecular back scatter an expected laser frequency spectrum of the order of KHz can well approximate a monochromatic source. Also, the radiation will be polarized to a high degree by the use of Brewster optics, which reflects light with a polarization angle different from the Brewster angle. The wavefront will also be plane when leaving the laser, but atmospheric turbulence will then degrade the wavefront. This can present a problem, but it can be shown that the effect in our case is negligible since the wavelength is relatively large and most of the return is expected from the first hundred meters[20].

2.2 CALCULATION OF THE EXPECTED RETURN

To maximize the scattering volume and thereby the returned signal, identical transmitting and returning paths (Figure 5) were used. This will of course mean that the returned signal represents a mean state of the atmosphere weighted as $1/r^2$. In a system used for actual sensing and not, as here, to prove a theory, one should use a pulse technique or a search light technique to achieve spacial resolution or as might be possible with stimulated M-B scattering a focusing technique. To determine the returned energy consider Figure 5.

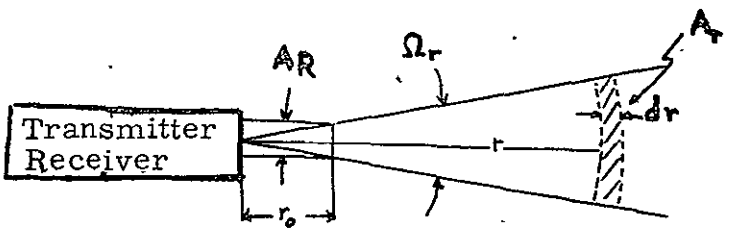

Figure 5. Homodyne detection using identical transmission and receiving optics.

In the volume element $A_r dr$ there are $N(r)\, dr\, A_r$ molecules with scattering cross section σ. The power per unit area, neglecting previous attenuation of the beam will be P_t/A_r, where P_t is the total transmitted power. The scattered light intercepted by the receiver aperture A_R from this volume is $A_R/4\pi r^2$. Thus for the return power $P(r)$ from the volume element we get,

$$P(r) = \frac{P_t}{A_r} (N(r)\, A_r dr)\sigma \frac{A_R}{4\pi r^2} \tag{48}$$

The total scattered energy P from the whole cone is,

$$P = \sum_{r_o}^{\infty} P(r) = \frac{P_t N(0)\, A_R \sigma}{4\pi} \int_{r_o}^{\infty} \frac{1}{r^2} dr = P_t \frac{N(0) A_R}{4\pi r_o} \tag{49}$$

In (49) the density variation with height is neglected since the decrease of this quantity with height is negligible compared with $1/r^2$. For the detection technique to be used - homodyne detection - it can be shown that those light waves originating within the Rayleigh range, r_0, are not sufficiently planar to be detected properly. The Rayleigh range is defined as the distance where the diffraction spread $r_0^2 \Omega_r$ from the original aperture is approximately equal to the original aperture A_R as shown in Figure 5, thus,

$$r_0 = (A_R/\Omega_r)^{1/2} \tag{50}$$

It can furthermore be shown[22] that for efficient homodyne detection to occur it is necessary that,

$$\lambda_o = (A_R \Omega_r)^{1/2} \tag{51}$$

The cross section of the beam exiting the amplifier was about 1 cm^2 which yields $\Omega_r = 10^{-6}$ steradians and $r_o \sim 30$ cm. With the two above

conditions the expression for the expected return becomes:

$$P = \frac{P_t\ N(0)}{4\pi}\ \sigma\ \lambda_o \qquad (52)$$

By using a gaussian profile[23] for the power distribution in the beam instead of an uniform one as we have done here it can be shown[22] that the return is times larger thus:

$$P = \frac{P_t N(0) \sigma \lambda_o}{4} \qquad (53)$$

The return per unit frequency $P(\omega_o)$ at the center of the M-B satellites is:

$$P(\ ') = \frac{P_t\ \lambda_0 R(\pi)}{4\pi \delta\omega_{MB}}\ \frac{7}{10} \qquad (54)$$

where $R(\pi)$ is the volume cross-section for backscattered light identical to that for Rayleigh scattering. The factor 7/10 accounts for the energy distribution of the three peaks. The two MB satellites overlay each other if one uses a beat detection system and organized atmospheric motion is negligible. The following is a list of representative values for our system.

$$R(\pi) = 1.68\ 10^{-12}\ cm^2$$

$$\lambda_o = 10.6\ 10^{-4}\ cm$$

$$d\omega_{MB} = 2\pi MHz$$

$$P_t = 50\ watt$$

With these values the expected return per unit frequency becomes:

$$P(\omega')\quad 10^{-22}\ watt/Hz$$

The minimum detectible signal for the technique we are to use-homodyne detection - is measured to be 7.6×10^{-20} watt/Hz[24], thus the signal to noise ratio in our case becomes,

$$S/N = 10^{-22}/7.6\cdot 10^{-20} \sim 10^{-3} \qquad (55)$$

This minute S/N ratio necessitates the use of signal integration, which improves the instantaneous S/N ratio above by the factor $(\Delta f.t)^{1/2}$ where Δf is the frequency interval the signal is integrated over, and t is the integration time. Using a receiver with a bandwidth of 600 KHz one gets.

$$S/N_{int} = 2.5 \text{ for } t = 10 \text{ sec}$$
$$S/N_{int} = 4.2 \text{ for } t = 30 \text{ sec} \qquad (56)$$

These S/N_{int} ratios justify an experiment, but special precautions must be made to achieve stability during the integration time. In the next section we will describe the experimental set-up used. In the previous discussion we have neglected absorption of the laser light. This is certainly justified since the return in our case will mainly come from the first hundred meters and the absorption at CO_2 laser light is only about 6% in the first kilometer[25].

CHAPTER 3

INSTRUMENTATION

3.1 INTRODUCTION

The previous analysis has revealed that the key requirements of the CO_2 laser system to be used are high output power, which is necessary for an acceptable signal to noise ratio, and high optical quality. This should include a narrow frequency distribution since a broad distribution would mask the frequency structure of the returned light, and also a single mode - single frequency laser system, since several transitions and/or modes would beat and result in erroneous features in the frequency analysis. The amplitudes of the local oscillator and the total power output must both be very stable, since variations in the amplitudes of these signals would make it impossible to properly integrate the return signal in time. It is furthermore obvious that the sensitivity of the detection system is a critical factor. The above requirements made it necessary to select a system with a laser oscillator (with a single frequency, single mode, but relatively low power output) followed by a laser amplifier (increasing the amplitude but not changing the frequency properties of the injected light). The power of a laser oscillator can realistically only be increased by increasing its length; this length is however limited to less than six feet by the requirement of a single frequency output. In the following sections we discuss the actual design of the laser oscillator, amplifier, and detection system.

3.2 LASER OSCILLATOR

The main causes of variation in the physical length of the cavity are variation in the length of the construction holding the mirrors, vibrations, and variations in the shape and thickness of the reflecting mirrors.

The construction holding the mirrors will change length because of temperature variations, and this effect was minimized by using low thermal expansion bars made from invar (expansion coefficient of about 10^{-7}/F).

Vibrations may be of either external origin, primarily caused by sound waves and building movements, or of internal origin arising mainly from bubbles in the cooling water. To minimize the effects of external vibrations the cavity was made heavy and sturdy by the use of four 10"x 10"x1" steel plates into which the 1" diameter invar bars were fastened (Figure 6). The whole system was furthermore placed on a 5 ton reinforced concrete slab which in turn rested on nine inflated truck inner tubes. (Figure 7). This arrangement effectively uncoupled building vibrations of typically 10-13 Hertz since the slab had a natural frequency less than one fifth this figure. Vibrations caused by sound waves were minimized by enclosing the whole oscillator in a lucite box surrounded on the sides and top by a 6" thick layer of sound absorbing tile (Figure 7). Vibrations caused by the cooling water for the laser tube were minimized by uncoupling the tube from the laser cavity by an external mirror system with the tube suspended by foam blocks which absorbed tube vibrations (Figure 8). The effects of bubble, and pressure fluctuations in the cooling water were minimized by a pressure head. All mirror holding constructions were made sturdy, (Figure 9) and attempts to minimize oscillations in the necessary spring loaded mirror holding systems were made.

Changes in the reflecting mirrors were caused primarily by heating from absorption of laser energy. These variations were minimized by the use of water cooled mirrors (Figure 9) made from silicon which combines a very low thermal expansion with good thermal conductivity. The

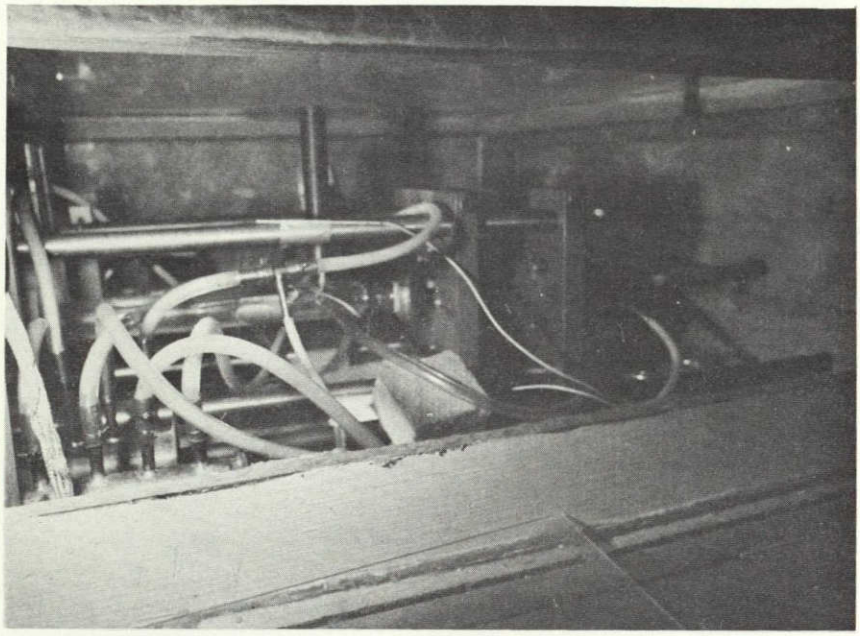

Fig. 6. - Support for the adjustable mirror.

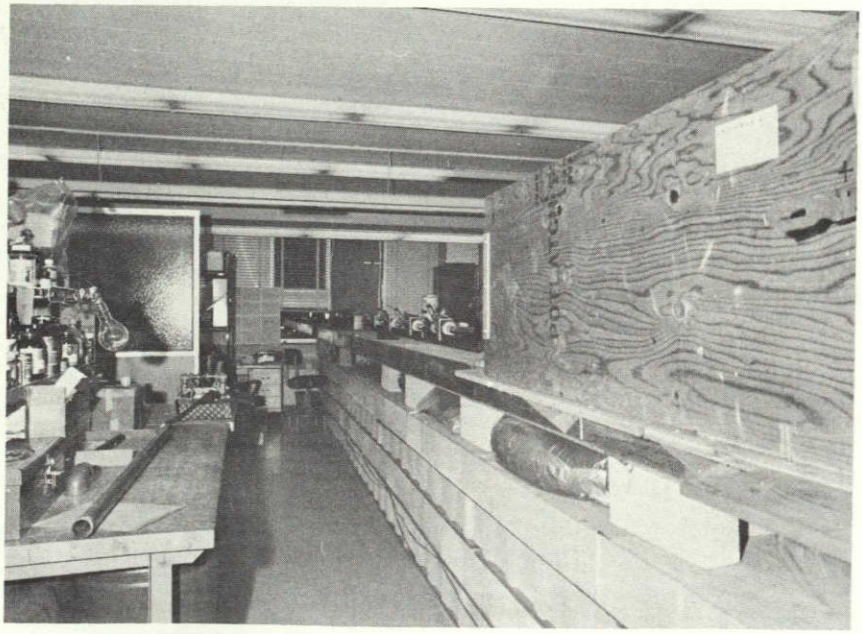

Fig. 7. - Optical bench and acoustic enclosure for the oscillator.

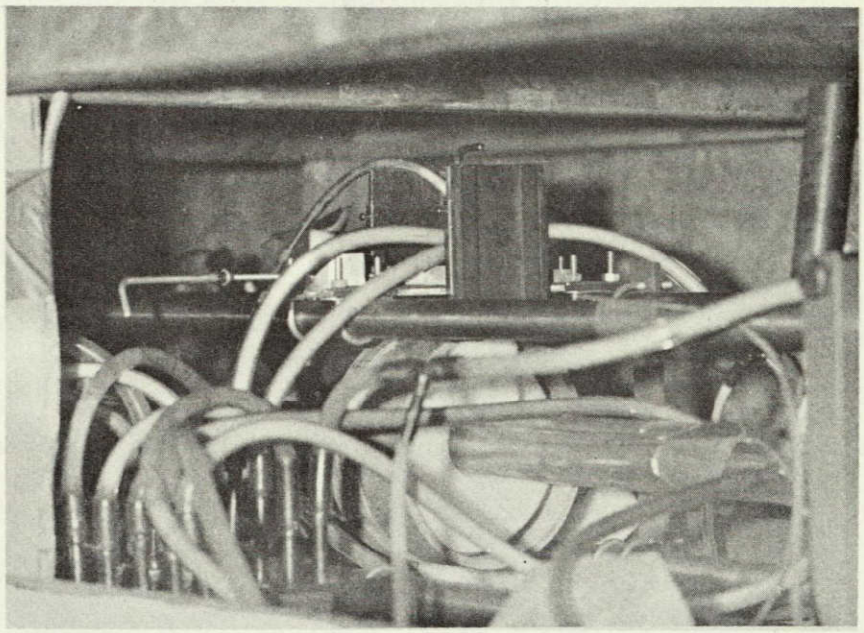

Fig. 8. - Discharge tube support for the oscillator.

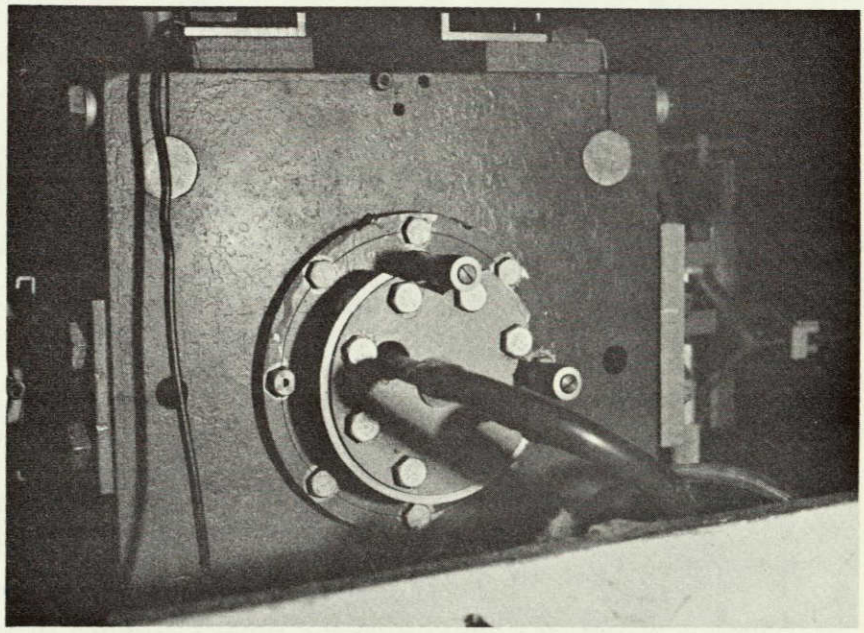

Fig. 9. - Mount for the fixed mirror.

mirrors were coated with a special highly reflecting gold alloy to further decrease the possibility of mirror heating.

The actual design of the laser oscillator is shown in Figures 10 and 11.

Variations in the index of refraction are produced primarily by partial as well as total pressure fluctuations, and changes in the discharge current. Total pressure fluctuations were minimized by using a large vacuum buffer system preceding the vacuum pump (Figure 12). Variations in partial pressure were eliminated by using premixed gas (10% CO_2, 15% N_2 and 75% He). Fluctuations in the discharge current were minimized by a line voltage regulator which compensates up to a $\pm$ 10% variation in the line voltage; a DC power supply to avoid the 60Hz AC modulations (34mA, 20 KV); a ripple filter attenuating a 3% AC ripple to an acceptable 0.03%; and an active current stabilizer which compensates for impedance variations in the discharge in the gas (Figure 13). Rather than using two electrodes and gas connecting parts, a high center electrode and two end electrodes combined with one gas inlet at the center and two outlets at the ends were used; this configuration reduced the voltage drop and the pressure gradient in the tube and probably also the adverse variations in these parameters. Large ballast resistors were also placed on the ground side of the discharge loop over which half of the voltage is dropped. These resistors were partially adjustable so that the amperage in both legs of the discharge could be equalized.

The adverse effect of changes in the optical length of the laser cavity are amplified if the new cavity configuration allows new modes and/or transitions to oscillate. To minimize this effect it was necessary to align the mirrors precisely and ensure that the oscillating frequency was

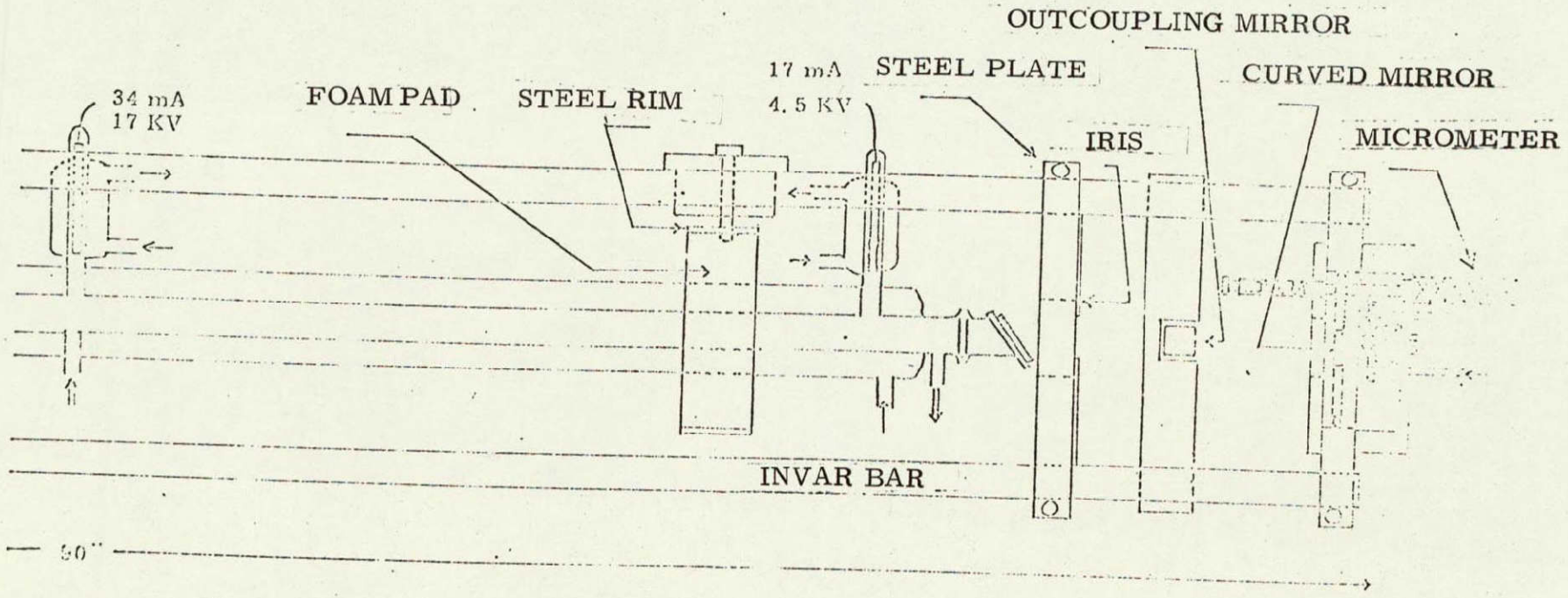

Figure 10. The Laser Oscillator

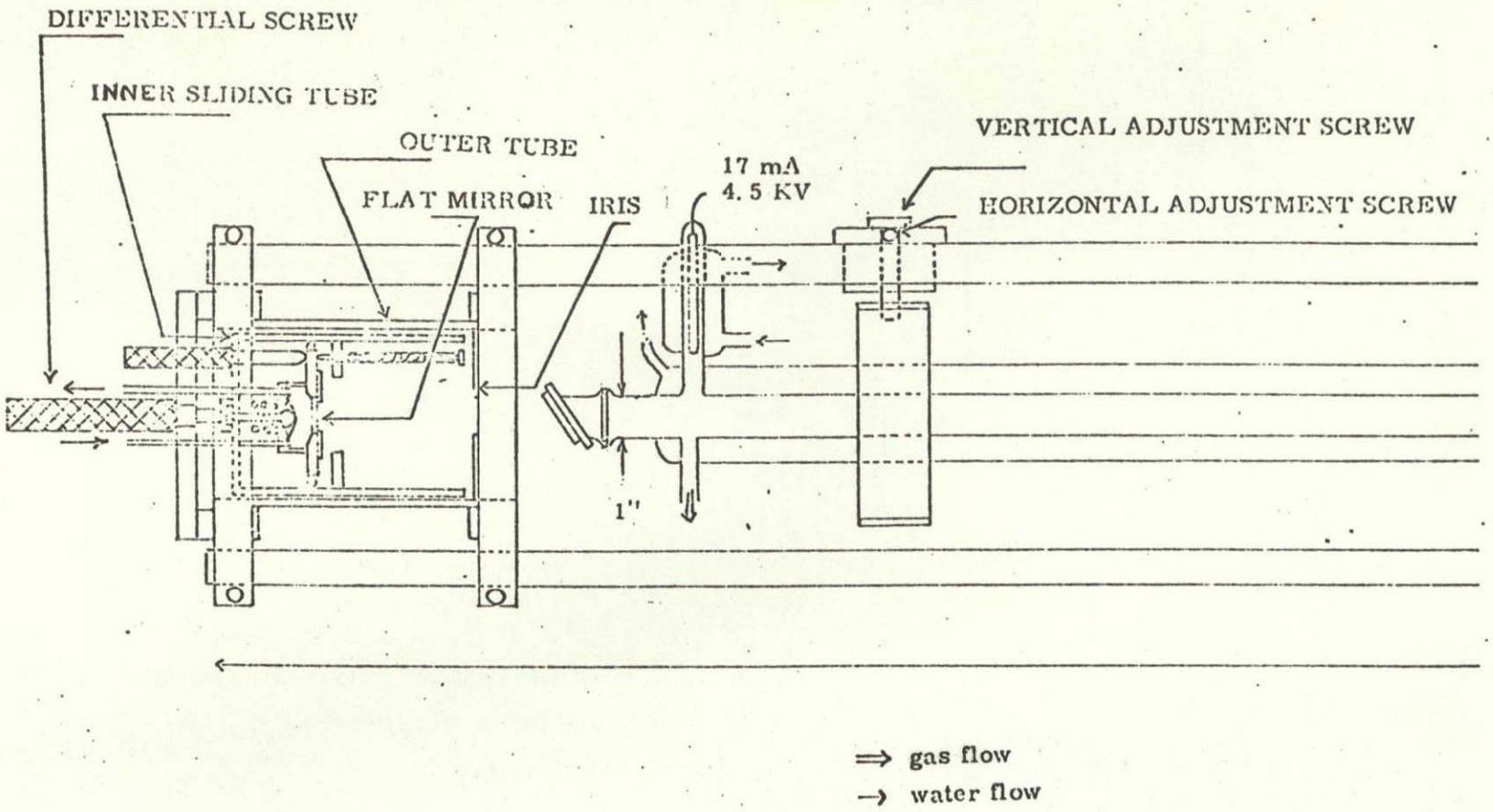

Figure 10. The Laser Oscillator

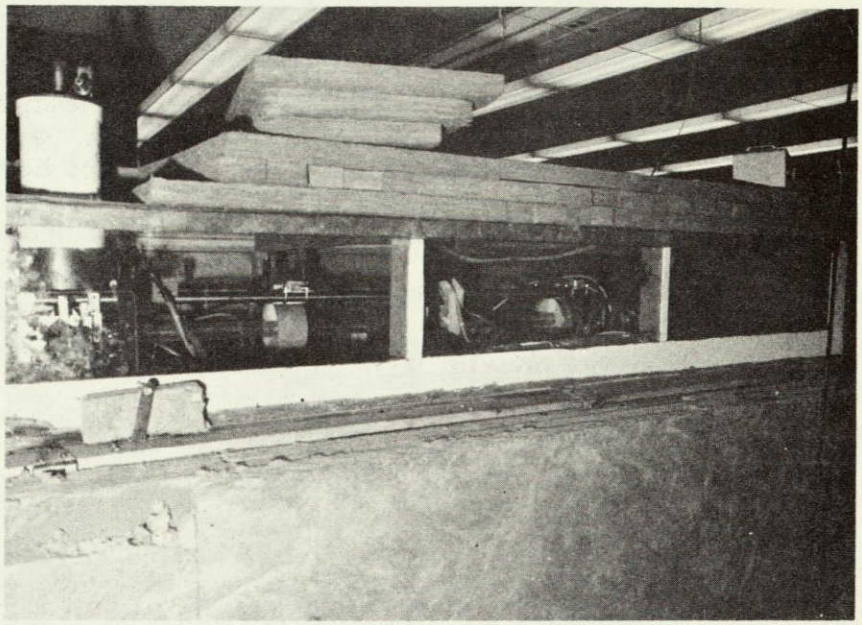

Fig. 11. - Laser oscillator and detector.

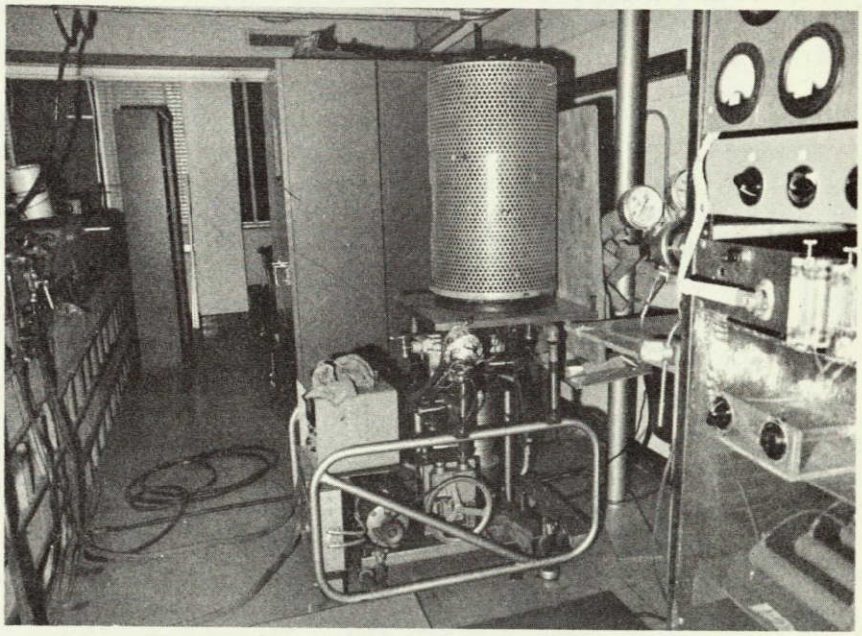

Fig. 12. - Vacuum system.

close to the center of a major transition gain curve. In order to attain this precision alignment, it was necessary to move the mirrors in two perpendicular planes independently of each other. The horizontal motion associated with this adjustment should also be maintained at a minimum; the actual design satisfying these requirements is shown in Figure 10. To further decrease the possibility of unwanted mode oscillations the following precautions were taken: a 30% reflecting mirror (15% in each direction) which produced a strong outcoupling, was placed in the path of the beam; the cross section of the oscillating beam was limited by irises adjusted so that only the lowest order horizontal mode could oscillate; and a folded confocal mirror configuration which discriminates against higher order modes was used.

To set the oscillating frequency to the center of the transition gain curve, one of the mirrors was moved by a differential screw (Figure 14). The centers of two consecutive gain curves for a six foot laser cavity are separated by about 25 MHz which corresponds to half a turn of the differential screw. Changes in alignment of the mirror during horizontal motion were prevented by attaching the mirror and its alignment micrometers to a one foot length of tubing which in turn moved inside a slightly larger tube. The laser tube could also be adjusted horizontally and vertically to further reduce the possibility of off-axis modes (Figure 8). The light emitted by the laser was polarized by the use of Brewster windows sealing the discharge tube (Figure 15).

3.3 LASER AMPLIFIER

The laser amplifier consists of two consecutive 18' long sections (Figures 16 and 17). The diameter of the first 9' section is 1" with the

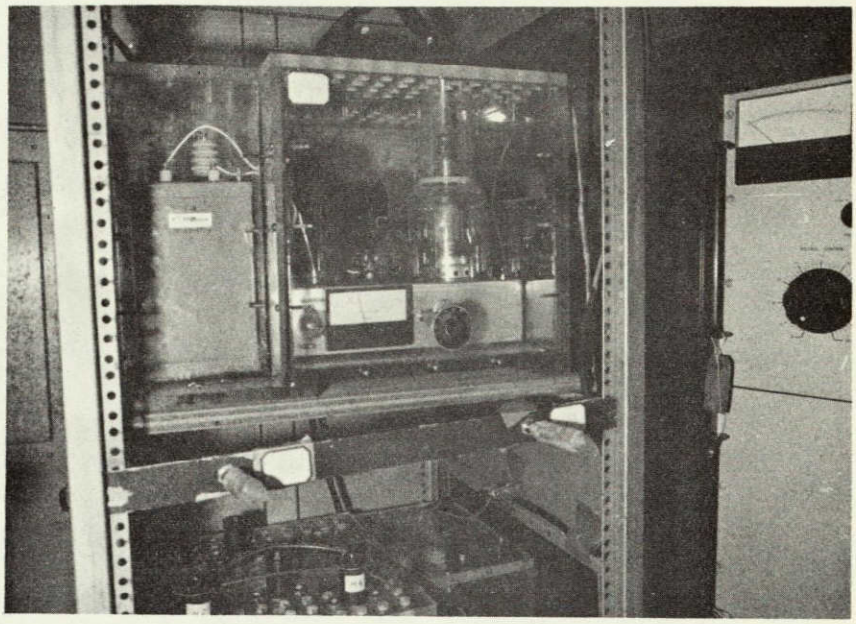

Fig. 13. - Current stabilizer.

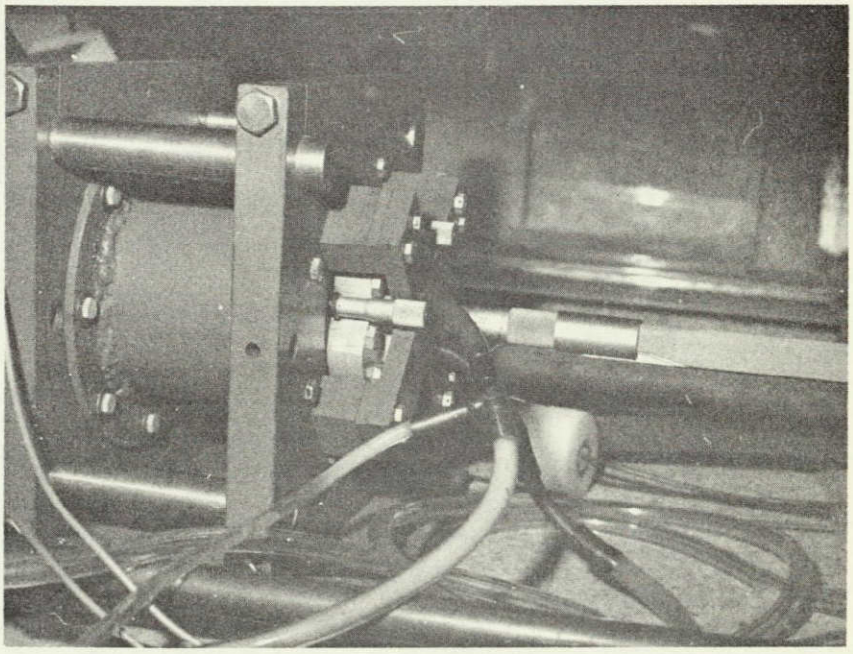

Fig. 14. - Differential screw.

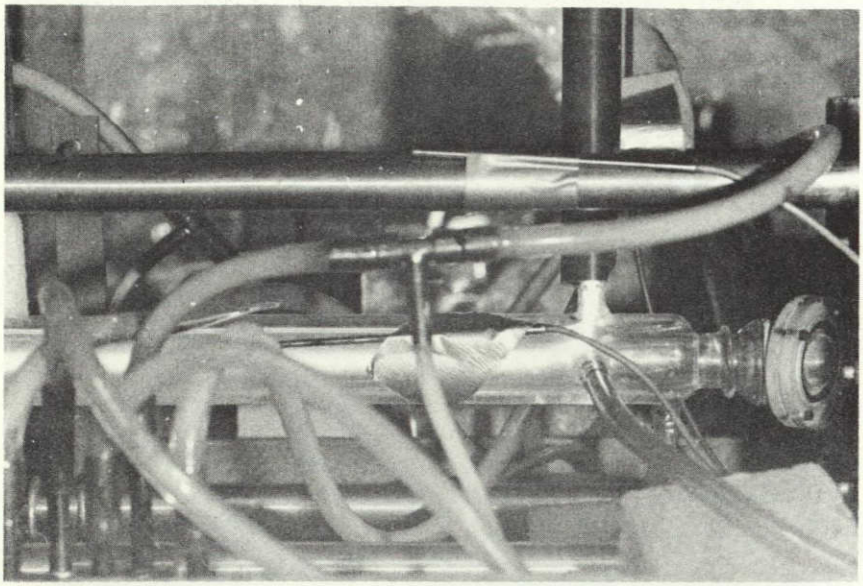

Fig. 15. - Brewster angle window for the oscillator.

Fig. 16. - Laser amplifier and optical bench.

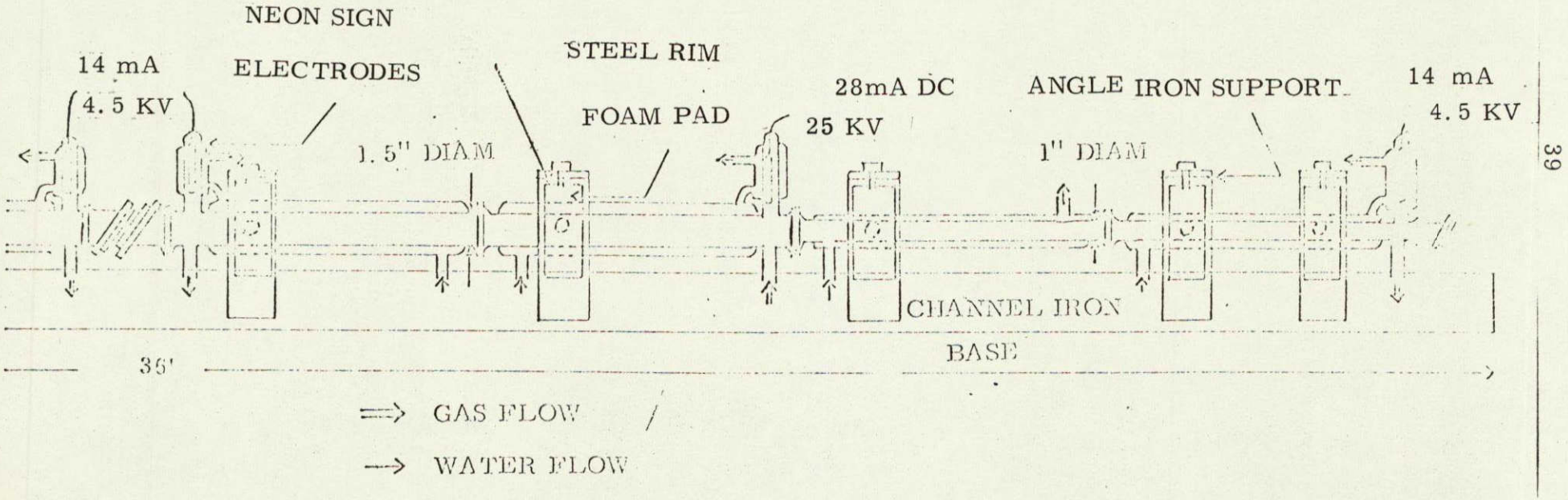

Figure 17. Laser amplifier. Section one, adjacent to oscillator.

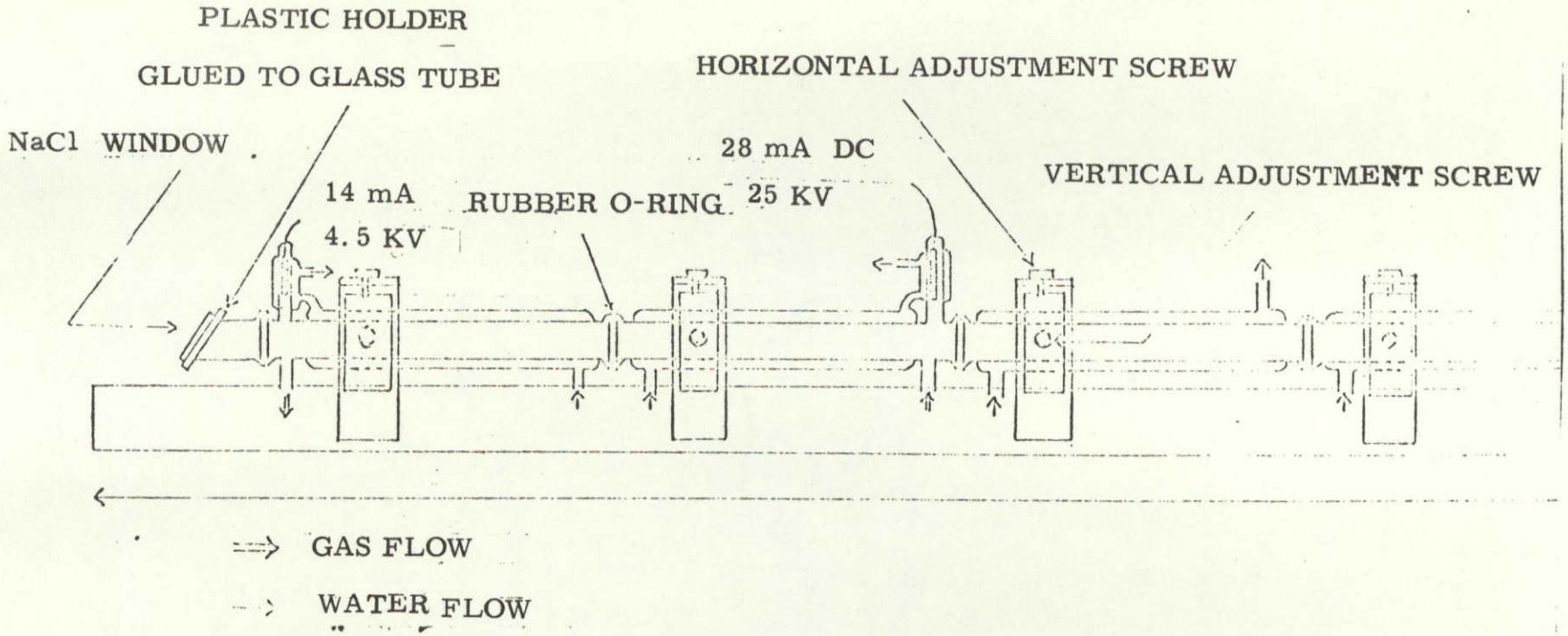

Figure 17. Laser amplifier. Section two, exit towards atmosphere

remaining being 1 1/2". This diameter configuration is a compromise between a larger diameter which permits easy alignment, and a smaller diameter which gives a higher gain. The amplifier is held by ten foam lined steel rims which in turn can be moved horizontally and vertically about supports bolted onto the 36' long steel channel along which the amplifier is mounted (Figure 18). The discharge tubes and the electrodes are watercooled and the amplifier has Brewster windows. The discharge system for the amplifier is identical to that for the laser oscillator except that a larger power supply is needed (60 mA and 30 KV). The amplifier used the same gas supply and vacuum system as the oscillator. Since the spherical parts of the oscillator beam reflected from the walls of the amplifier, it was necessary to collimate the beam with a mirror of the same curvature as the curved mirror of the oscillator itself. The laser amplifier increased the 5 watt output of the laser oscillator to about 45 watts; the efficiency of the laser oscillator and amplifier was about six percent. The short term output was very stable, but a long term drift ($\sim$10 min) of the output power could not be avoided. The power output of the amplifier was monitored by reflecting a small portion ($\sim$2%) of the beam into a laser power meter (Figure 19). After leaving the amplifier the beam passed through an opening in the wall to the outside where after approximately 8', a 45^{o} gold coated mirror reflected the beam into the atmosphere.

3.4 DETECTION SYSTEM

The detection system used is shown in Figure 20. The return signal, retracing the path of the emitted beam, goes first through the laser amplifier where the power is increased by about one order of

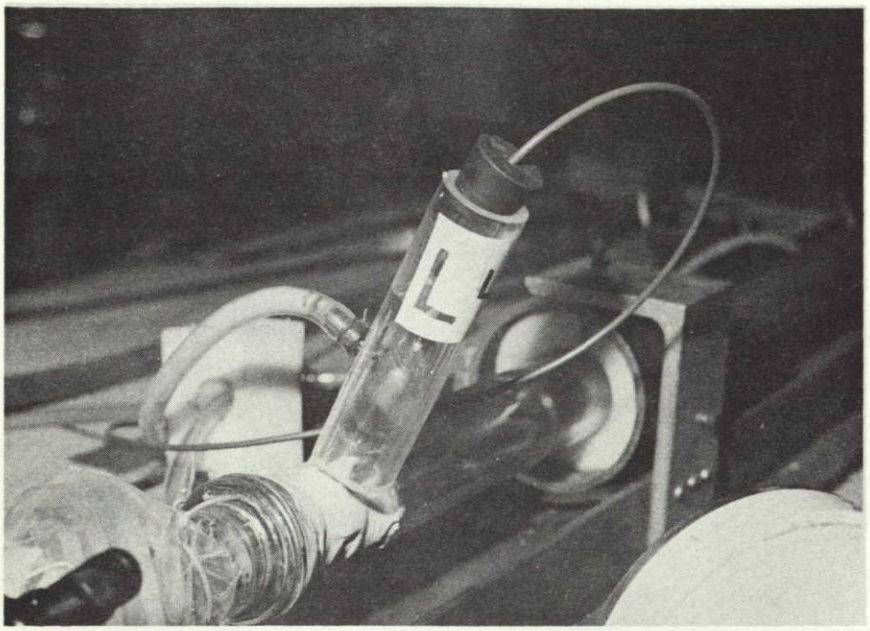

Fig. 18. - Amplifier electrode and support.

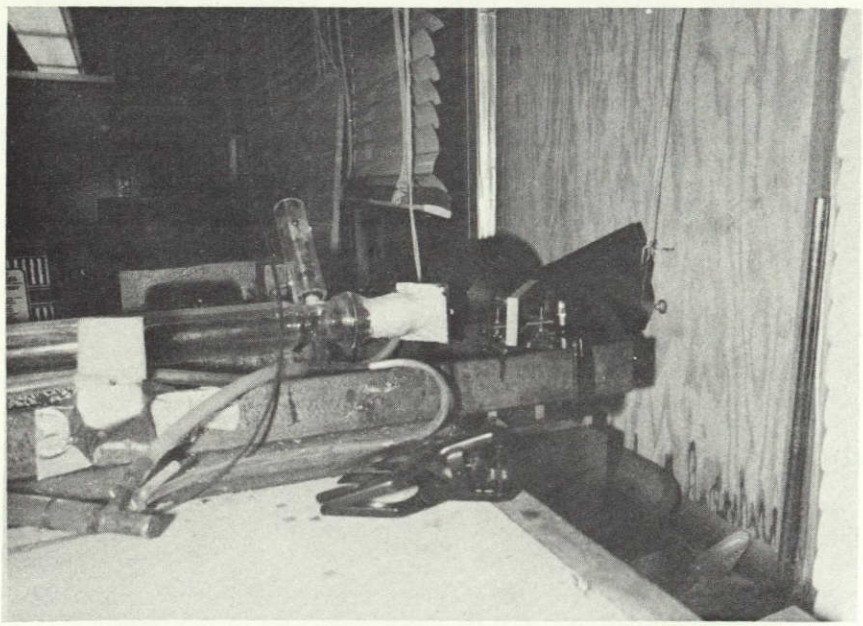

Fig. 19. - Choppers and power meter head.

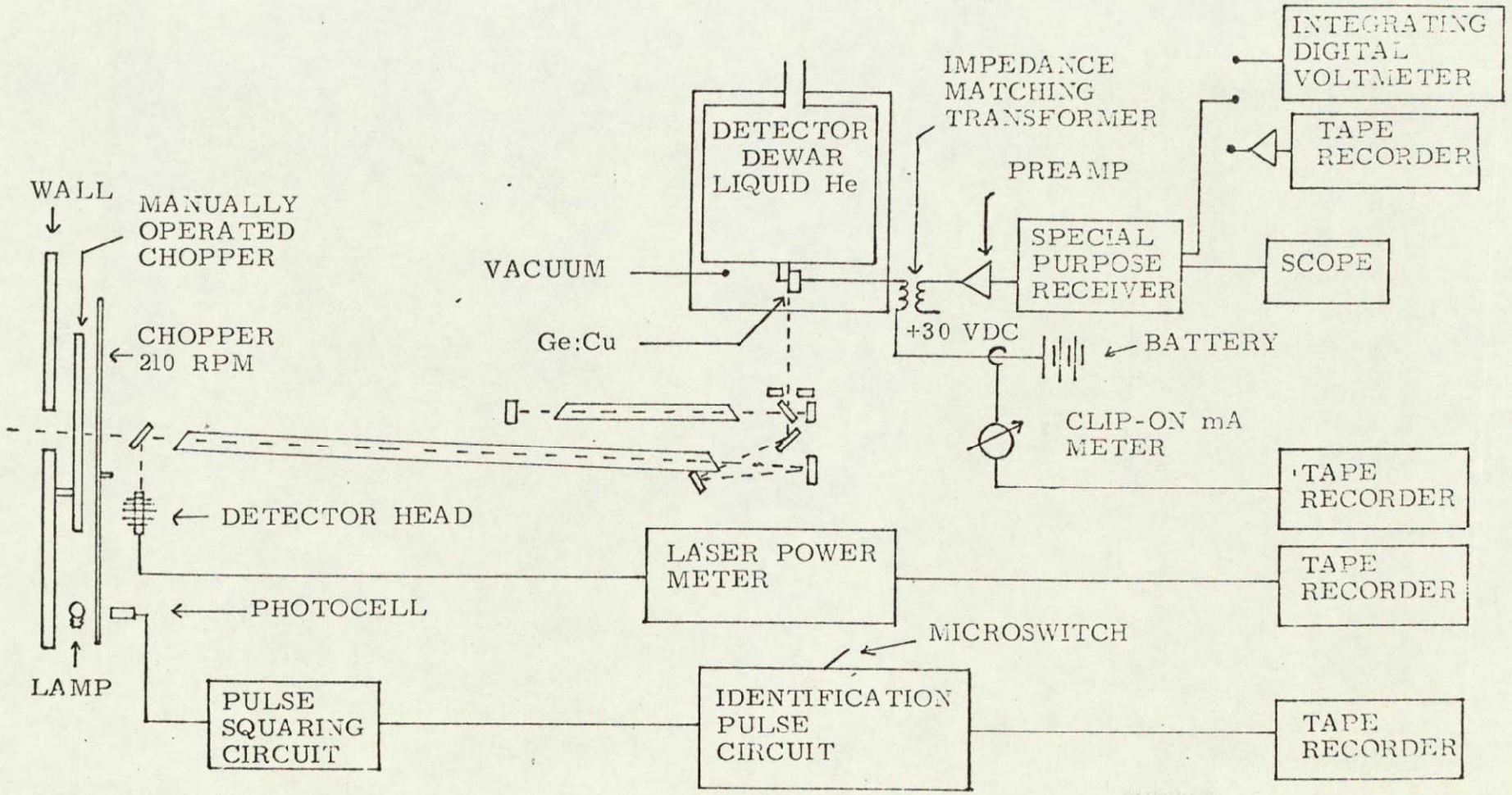

Fig. 20 .- The detection circuit.

magnitude; however, while spontaneous emission in the amplifier tube is increased by the same amount, the signal to noise ratio will not increase significantly. After a loss of about 15% at the outcoupling mirror, the return signal is joined by the local oscillator signal, and it is here that the signal to noise ratio is established. After passing through the aperture in the coated saltmirror (see Figure 21) the two beams are reflected onto the detector element by a 45^{o} mirror (Figure 22). The detector element (Figure 23), responding to the square of the total incoming power, "mixes" the two signals and the photocurrent generated in the element will therefore have a component with a frequency corresponding to the difference in frequency of the two signals i. e. a beat frequency signal. Mathematically, this process is as follows; let the local oscillator signal and the return signal be given by,

$$P_{lo} = A_{lo} \cos\omega_{lo} t$$

$$P_{s} = A_{s} \cos\omega_{s} t$$

When these two signals beat together on the detector face the generated photocurrent, I, is given by,

$$I = (P_{lo}+P_{s})^{2} = A_{lo}^{2} \cos^{2}\omega_{lo} t + A_{s}^{2}\cos^{2}\omega_{s} t + \frac{1}{2} A_{lo}A_{s}\cos(\omega_{lo}+\omega_{s})t + \frac{1}{2} A_{lo}A_{s}\cos(\omega_{lo}-\omega_{s})t$$

All except the last term in this expression appear as DC signals since their optical frequencies are much too high to be registered by the subsequent detection electronics. These electronics will therefore see a large DC component (mainly from the first term on the right side in the expression above) with a small AC signal superimposed. To maximize the signal to noise ratio the noise generated in the detector (generation-recombination noise) is made the major noise source in the detection system by using a strong local oscillator signal. To reduce thermal

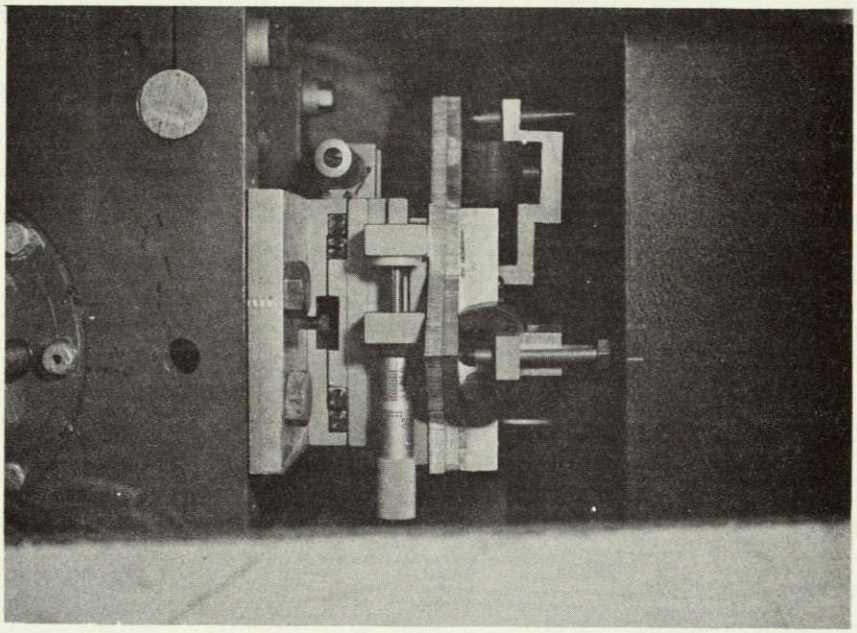

Fig. 21. - Mirror mount for the mirror with an aperture.

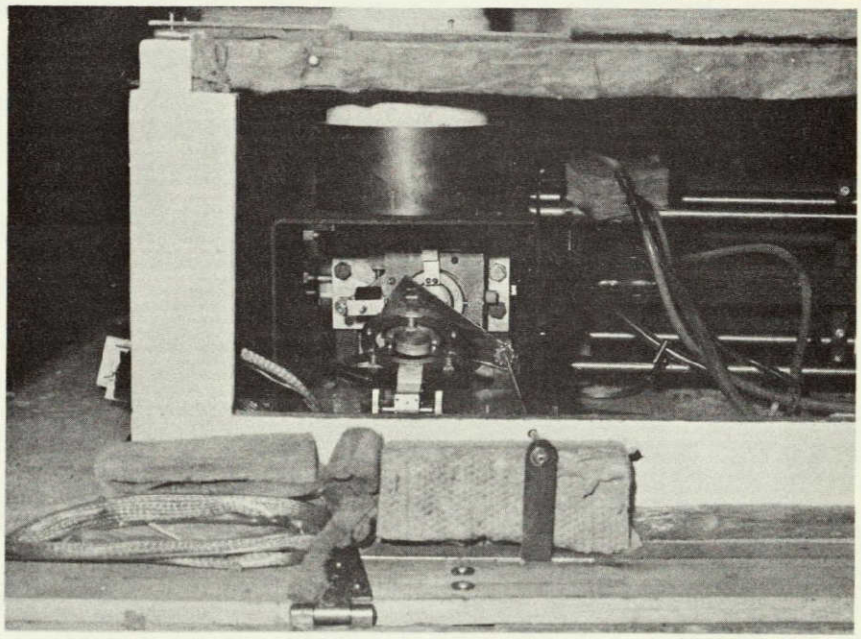

Fig. 22. - Holder for the 45° mirror.

noise to an acceptable level the detector element was cooled to 4K by liquid helium. The detector was biased by a DC voltage to increase its sensitivity.

The output from the detector element was fed through an impedance matching transformer via a preamplifier to a special purpose heterodyne receiver which in turn produced DC output proportional to the incoming VHF signal (Figure 24). The receiver had a frequency response of 55 to 200 MHz and a maximum bandwidth of 600 KHz. The receiver output was subsequently treated in a number of ways which will be described in the next section. To investigate possible variations of the local oscillator power which was reflected by a change in the bias current, a clip-on milliammeter monitored the bias.

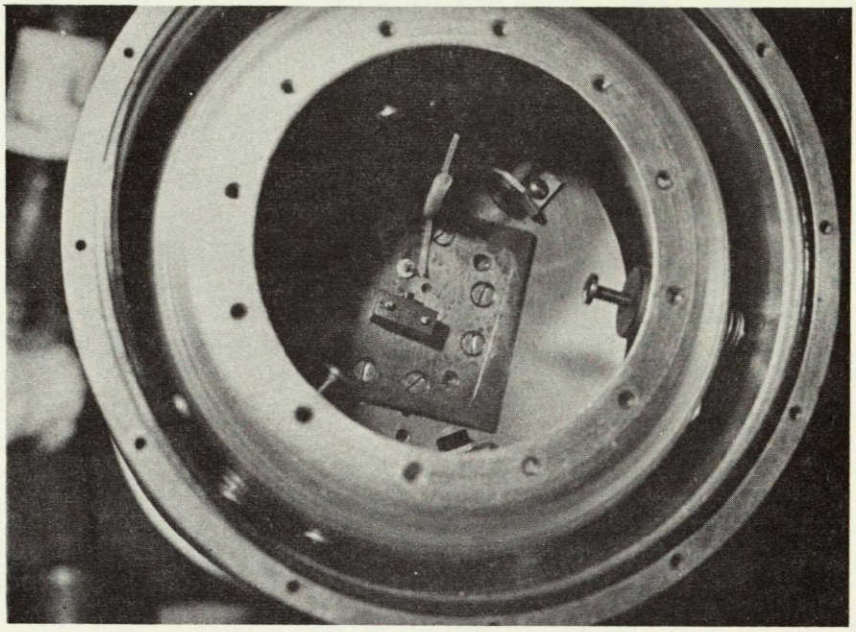

Fig. 23. - Detector element in dewar.

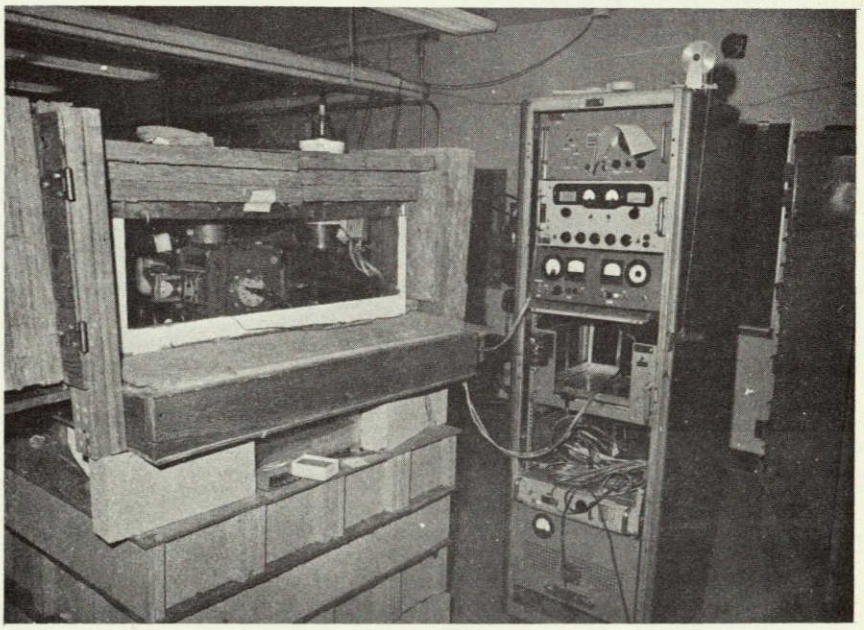

Fig. 24. - Electronics for the detection system.
In the rack from top: Scope, receiver, battery box, amplifier power supply, digital voltmeter, amplifier and line voltage regulator.
On the bench: Laser power meter.

CHAPTER 4

DATA COLLECTION AND ANALYSIS

4.1 METHODS OF DATA COLLECTION

Four different procedures for compiling the experimental data were used, the purpose being to develop a method whereby the signal noise could best be subtracted from the received signal. In addition the dark response (i.e. the response without laser power on the detector) was determined from a series of runs made with various bias currents, the results of which are shown in Fig. 25. These procedures and the results for each are presented below.

Digital integrating voltmeter - power meter

In this arrangement the low frequency output of the receiver (proportional to the VHF input) was fed to an integrating digital voltmeter set to an integrating period of 20 seconds. A run was first made for the laser beam entering the atmosphere. For every second frequency setting (600 KHz width) between 55 MHz and 81 MHz the integrated voltage for five consecutive periods was recorded and later averaged. After the run was completed a similar run followed, but the laser beam was now blocked from the atmosphere by the laser power meter. Integrated voltages were collected as in the prevoius run. This run was then followed by an additional unblocked and blocked runs. The two types of runs were separately averaged for each frequency and the result is shown in Figure 26. The difference in return between two consecutive runs was for each frequency normalized by the chopper return (Figure 27). The fluctuations in the absolute returns during the first two runs with this arrangement (Figure 26) were rather large and might have been caused by drifts in the output power and

the laser oscillator power.

Recorder, computer - rotating chopper

To reduce effects of long term drifts which were apparent in the preceding method, a scheme was introduced using a rotating chopper which periodically (with a 70 msec period) blocked the beam from the atmosphere. The chopper was coated by black velvet paint to minimize reflections. The position of the chopper was recorded on magnetic tape together with the continuous low frequency output of the receiver. The recorded data were subsequently processed by a hybrid computer which could be set to calculate the average integrated return with: the chopper blocking the beam from the atmosphere; the beam entering into the atmosphere; and the chopper first blocking the beam, then subtracting the integrated return from the following unblocked period.

A signal could be made to override the chopper position signal and mark a change in the frequency setting of the receiver. This signal terminated the averaging process, printed the result, and initiated the averaging for the next frequency. The result from one run is shown in Figure 28, where the average returns with the beam blocked and with the beam entering the atmosphere are plotted for each frequency during the run. The units on the ordinate are volt sec although the magnitudes are relative. From such plots it was obvious that the returns had to be normalized to counteract non-linear detector response. This normalization was done by dividing the unblocked atmospheric return, A, with the return recorded with the chopper blocking the beam, C ; this ratio will be referred to as A/C. The calculated difference, D, was normalized in the same way, referred to as D/C. For four of the eight runs made, D/C is plotted in

Fig. 29. Fig. 30 and 31 show the average A/C and D/C for these eight runs.

The smooth absolute returns for these runs indicated that the effects of long term drifts were reduced. However, it was suspected that the rotating chopper could have a modulating effect on the returned signal causing erroneous features. The appendix gives a detailed description of the data collection and processing for this scheme.

Digital integrating voltmeter - manual chopper

To investigate possible modulating effects by the rotating chopper on the returned laser light, a set of runs were made with the rotating chopper replaced by a manually controlled chopper which blocked the beam every second 20 sec. interval. This chopper was also coated with black velvet paint to reduce reflection. The low frequency voltage from the receiver was integrated by the integrating digital voltmeter and recorded. Five runs were made in this manner and the results are shown in Figure 32 where the voltages for the blocked and the unblocked periods as well as the difference, normalized by dividing by the chopper return, are plotted. From the results of this run it was apparent that modulation by the rotating chopper did not cause erroneous signals since the main features were repeated in this run where no rotating chopper was employed. It was furthermore hoped that the combination of the manual and the rotating chopper would further enhance the reliability of the conclusions.

Recorder, computer - rotating and manual choppers

To further ensure that the observed features in the returned signal were caused by variations in the scattered light the final procedure included both the rotating and the manual choppers. The received signals were processed as described for the August runs. A run was first made

in the same manner as in the August runs, followed by an identical run except that now the manual chopper blocked the beam. This technique was employed on two occasions, November 3 and 5, and 29 and 30. Altogether eight unblocked and five blocked runs were made. The average results for A/C and D/C are shown in Figures 34, 35 and 39, 40. The average ratio between A/C for the unblocked runs and that for the blocked runs is plotted versus frequency in Figures 35 and 42. The corresponding ratio for D/C is plotted in Figures 36 and 41. The arrangement with both the rotating and manual choppers further clarified the primary features in the return and again disproved the suspicion that the rotating chopper had an adverse modulating effect on the return. It was therefore concluded that this arrangement was superior to the other procedures.

4.2 SOURCES OF ERRORS

Major noise sources that contribute to uncertainties in the data are: the non linear response of the receiver, impedance mismatch, resonance-antiresonance effects in the transmission lines, variations in the output power caused by frequency drifts in the laser oscillator, mirror vibrations, and,less severe, electronic drifts in the analog section of the computer. These are discussed below, along with the methods used to minimize the noise.

i. Receiver.

With an open antenna the receiver did have a very non linear response (see Figure 25) which could have contributed to the observed peaks in the returns in e.g. Figures 28 and 38. The frequency response curves for the runs with the detector in the system but no laser light reaching the element (see Figure 25) exhibit much the same pattern as those with light reaching the detector, although the absolute value of the return signal in this latter case is about 10-20% larger.

ii. Transmission lines.

Difficulties such as impedance mismatches, and anti-resonance and resonance in the transmission lines caused by a build-up of standing waves probably contribute to the non linearity of the returned signal. For instance, at 72 and 63 MHz a standing wave would have a wave length of a multiple of 0.687 m and 0.786 m respectively. Since the cables used were 2.9 m (receiver), 1.54 m (bias), and 1.61 m (amplifier power), such standing waves could have developed causing differential amplification of the return at 68.2 MHz (a half wave for the bias line) and at 61.4 MHz (a half wave for the amplifier power line). The non linear behavior did not change significantly at these frequencies

when the antenna line was disconnected, which reduces the probability of serious adverse effects from this source of error.

iii. Laser Oscillator

Long term drifts in the net output power (of the order of 10 min) of up to 20% were observed during some of the runs. Although the power could easily be regained by moving the differential screw (Figure 14) to recenter the oscillating frequency to the center of a gain curve, this was generally only done after a complete run to avoid a change in the lasing frequency and sudden jumps in the return caused by an increase in laser and local oscillator power. This drift did present a problem during some of the experiments but normalization of the data reduced these adverse effects, and, in addition, averaging over several runs resulted in further reduction. For time periods of the order of one minute the output power showed very small variations (less than one percent).

iv. Mirror Vibration

The mirror with an aperture through which both the local oscillator and the returned signal had to pass (Figure 21) was very sensitive to small motions, and though extreme care was taken to ensure rigidity of the mirror mount, vibrations of the mirror could cause variations in the return signal. Averaging over several runs should minimize the effects of these variations. Other mirrors, particularly the mirror projecting the oscillator beam through the amplifier, were also very sensitive to motions although to a lesser degree.

v. Computer

Some of the tapes were run several times to determine the effects of drifts and errors in the processing units. Though differences

from one run to the next were observed, these were not of such an order that they could impose erroneous features in the records. Averaging for a number of runs also minimized the errors. Other possible noise sources which were investigated and found to be of lesser importance are,

vi. Modulation of the return prior to detection

Modulation can occur by the rotation of the chopper or a selective frequency return by the chopper blades. If modulating effects by the rotating chopper would significantly contribute to the observed features in the return, these features would be absent in the runs where the rotating chopper was not employed (Figure 32). Since this is not the case it is concluded that modulation by the chopper did not significantly modulate the return signal. If the coating (3 M velvet coating #107 C10 Black) on the choppers selectively reflected the laser light then this could explain the return signal features. This explanation seems rather unlikely and is furthermore substantiated by tests conducted which show low extremely uniform reflectance with frequency[26].

vii Differential amplification

Differential amplification can occur in either the laser amplifier or cavity. The light returning through the laser amplifier was of course subjected to a gain determined by the gain curve for the transition used by the amplifier. This gain curve has a full halfwidth of about 50 MHz and transitions are separated by KMHz. It is therefore not possible to explain the variations found in the return signal by differential amplification in the laser amplifier. However, the sloping gain curve would cause a uniform change in the gain depending on which side of

the center of the gain curve the lasing occurred. This differential amplification (of maximum 2%/ frequency) could have resulted in a shift of a peak in the return of at most one MHz. Some of the returned light (about 15%) will enter the laser cavity and might go into oscillation causing a peak at the beat frequency between this return and the oscillating wave in the laser. This peak should however have a width about the same as that between modes of the main oscillation which is of the order of KHz and would thus appear as sharp peaks on the visual display. Since no such peaks were observed during the runs this noise source seems very unlikely.

viii VHF Interference

VHF interference can occur from a number of different sources. Though there are a number of TV channels and sidebands in the actual frequency spectrum (55, 59.5, 63.7, 71.8, 75, 83.2 MHz) these are much too narrow (about 100 KHz) to explain the several MHz wide peaks in the return. No such peaks were furthermore observed on the visual display. Also some of the tests were made at night when there were no TV signals, and no significant difference in the return was observed. It is therefore concluded that this interference did not appear in the detector and cause the observed features in the return. The above reasoning together with the fact that the discharge systems had filters which severely discriminated against VHF interference makes TV and radio interference with the laser system itself equally unlikely. VHF discharges from the high electrodes in the laser amplifier to the pump and tube supports were observed initially. These were subsequently eliminated by redirecting the gas flow (which was made to enter at the

high electrodes) and by coating the supports by corona dope, the discharges resulted in very sharp, easily observed peaks which occurred regularly in the observed frequency interval. These were not found after the above precautions so it was concluded that VHF discharges did not have an influence on the detection. Further possible sources of irregular VHF response in the detection system are the detector element, impedance matching transformer, and the pre-amplifier. Though it was not possible to test the frequency response of the detector element itself, it can safely be assumed (e.g. (27)) that there were no irregularities in the response causing the observed features in the returned light; however, a uniform decrease of the response with increasing frequency is to be expected. Also according to the manufacturer's specifications, the transformer performance does not exhibit any irregularities similar to those observed in the return, while the specification for the preamplifier is again curve centered at 60 MHz and 3 dB points of ($\pm$ 25) MHz which could not have caused any of the observed features in the return. Interference from the recorder and/or cables leading to it did cause a typical interference pattern which however was eliminated by placing the recorder in a shielded room.

Other sources of error entering the interpretation of the results are scattering previous to the chopper and uncertainty of the lasing wavelength. Scattering of laser light prior to the choppers would mainly have occurred along the path of the laser beam between the laser oscillator and the amplifier. However since the total power of the light in this path is an order of magnitude less than that from the amplifier

the effects of this scattering should be secondary. The chopper could of course have been moved to a position immediately following the oscillator, but such an arrangement would probably have resulted in adverse modulation effects of the power output of the laser amplifier.

Uncertainties in the frequency of oscillation can result in an instrumentally imposed variation of the shift of the returned light of up to 5 MHz. This would completely mask the variations caused by the actual temperature variation between the runs (about 1 MHz for a change of temperature of 20 ^{o}F). Table 2 lists transitions, thought to be powerful enough to have been selected when the laser was tuned to a major transition. The expected shifts in frequency for a sound velocity of 361 m/s[13] are also given.

Line	Branch	wavelength(μ)	Shift (MHz)
P (14)	$00^{o}1$-100	10.531	68.6
P (20)	"	10.590	68.2
P (26)	"	10.653	67.8
R (14)	"	10.288	70.2
R (20)	"	10.259	70.5
P (20)	$00^{o}1$-$02^{o}0$	9.552	75.6 (less probable)

Table 2. Expected frequency shifts for possible lasing transitions

It can be seen from this table that if the laser oscillated within the same P branch a possible variation of the returned frequency would be about 1 MHz, while a shift from a P branch to an R branch would result in a 2 MHz change in the frequency shift of the return.

CHAPTER 5

RESULTS, CONCLUSIONS, AND SUGGESTIONS FOR FUTURE WORK

5.1 RESULTS

In order to properly interpret the return signal, it was necessary to determine the dark response from the detector system (Figure 25). The non-linearities of the detection system are obvious for all the bias voltages, and do indeed make the returns difficult to interpret, particularly since the returns were only 10-20% above the dark noise value. One should note that there are two maxima in the noise, one at 72 MHz and the other at 62 MHz; this is rather unfortunate, since the expected returns from stimulated and spontaneous M-B scatterings are near these frequencies. There does not seem to be any distinctive relation between the value of the bias voltage and the variation of the peaks or the total response of the detection system. Possible sources for these non-linearities were discussed in section 4.2.

July Data

Results of the July 16 runs are given in Figures 26 and 27. The bias voltage for this set of data was 37 V. After the two first runs (atmosphere 1 and meter 1 in Figure 26)* the laser was tuned to regain power which unfortunately resulted in less light reaching the detector, and caused the bias current to drop from 10 mA for the first two runs to 7 mA for the last two. This explains the drop in the total measured intensity for the second runs. The absolute return (Figure 26) showed such large variations with frequency that it was decided for future runs to monitor the background noise more frequently in order to reduce the effect of long term drifts. The "meter" runs started at 55 MHz and ended at 76 MHz while the opposite was true for the "atmospheric"

*Meter 1 refers to the first run with the power meter obstructing the light. Atmosphere 1 refers to the first run with the light entering the atmosphere.

runs. For each frequency setting during the individual runs, data were collected for about twenty 20 second intervals and averaged to yield the curves in Figure 26. The first two curves and the second two have one thing in common, namely, the atmospheric return is greater than that from the meter runs, only in an interval around 70 MHz. This is even more apparent in the differences between two consecutive runs, and in the ratio between these differences and corresponding chopper returns (Figure 27), as well as the average curve for this ratio. This peak in the differences has a full width at half power (halfwidth) of about 5 MHz.

August Data

Different bias voltages were used for the August runs in order to determine possible effects on the return signal: 34V for the August 18 runs, 26V for the August 21 and two of the August 22 runs, 21V for the third August 22 run, and 14.5 V for the fourth August 22 run. This decrease in bias voltage from 34 to 14.5V reduced the absolute returns by about 10%, a behaviour that was not observed for the dark response for a corresponding bias change, Figure 25. The shapes of the absolute return curves all show reasonable agreement with the corresponding dark curves as exemplified by Figure 28. For example, the poorly developed peak around 61 MHz in the absolute return for the runs employing a bias voltage of 26V is evident in the dark response curve for the curve of the closest bias voltage of 24.5 V. The most striking feature in all the D/C* and A/C curves is a sharp signal at 61 MHz.

* For a complete discussion of these signal ratios, see appendix.

This signal does not generally coincide with a maximum in the total returns but occurs one to two MHz lower. The absolute value of this signal in the D/C (Figure 29) and A/C ratios increased markedly with each succeeding run and gives the appearance of a threshold effect. The second feature apparent in these curves is a signal around 69-70 MHz. This peak is less well developed than the aforementioned feature but occurs consistently in the runs, but with a variation in frequency from 69 MHz in the August 18 and 21 data, to 72 MHz for the August 22 runs. The halfwidth is about four to five MHz from the average D/C curve Figure 30. The average A/C curve(Figure 31)is centered at a higher frequency, 72 MHz, and shows three smaller peaks, which suggests that this increase in the width is caused by the averaging process.

It is concluded from this set of data that the absolute values of the return signal retrace the non linear behavior of the dark value curves - although at 10-20% higher absolute values. The normalization brings out two features present in the scattered light, a sharp return at 61 MHz and a broader less well developed signal at 69 or 72 MHz.

October data

The bias voltage used was 30 V in all of the eight runs. For each frequency setting, the signal was integrated with the manual chopper open for a period of 20 sec. followed by an integration period of the same length but now with the chopper closed.

The total returns (Figure 32) show the same behavior as those for the August runs - two large peaks roughly coinciding with those characteristic of the dark response curve. This is particularly obvious in the interval below 60 MHz where the 30 V dark curve is the only one

to show a sharp increase, a feature also present in the absolute return curve.

The difference between the two curves normalized by the chopper return in Figure 32, shows the same two features noted previously, a sharp signal at 62 MHz and a smaller, broader signal around 72 MHz, the halfwidth of which is about 4 MHz.

An important advantage of the digital integrating voltmeter, which was used in this set of runs, is that the absolute values of the returns can be compared. In the recorder-computer arrangement, an offset which effects positive and negative integration somewhat differently, had to be used, and this made the absolute values of the return less reliable. The offset did not alter the shape of the curves significantly.

November data

The bias voltage for early November data (Figures 33 to 37) varied from 26V for the first run to 21V for the last. Altogether, six runs were made with the manual chopper open and two with the chopper closed; these two runs each preceded three atmospheric runs (with chopper open). The absolute returns (Figure 33) are again similar to the dark response curves, but specific features between the return for individual runs and corresponding bias dark curves are more difficult to find. The 72 MHz peak in the absolute returns is well developed, while the return for the lower frequency is not so pronounced.

The average D/C curves (Figure 34) for the runs with the manual chopper open show a peak around 69 MHz, a feature not present in the runs with the manual chopper closed. This is the only interval where

the D/C (Figure 34)and A/C (Figure 35) ratios for the "manual chopper open" consistently are greater than those for the "manual chopper closed". The only other interval where these two curves are different is around 61 MHz, where the curves representing the return with the manual chopper closed are higher. A peculiar feature in both graphs for which no explanation is apparent is the large return signals for 55 and 56 MHz.

When the values for the returns with the manual chopper open are divided with those for the manual chopper closed, the two aforementioned features show up clearly (Figure 36 and 37) although less so for the 61 MHz signal. The peculiarity at 55-56 MHz does not show on this curve. It can therefore be concluded that the rotating chopper had a more pronounced effect on this feature than the manual chopper. The effect of the rotating chopper reverses the 61 MHz signal while the manual chopper increases the return signal as was the case for the October run. This reverse probably occurred because the chopper was realigned at an angle off axis to the laser light to minimize reflections from the chopper blade.

The late November runs are less reliable than previous runs because problems were encountered maintaining the laser output power and the local oscillator power; most of the runs had to be interrupted in order to realign the laser to increase the power. This problem had not plagued any previous runs to such an extent. Also some of the pulses which identify a change in the frequency did not register, making the data treatment more difficult. Because of the instrumental problems it was only possible to make two atmospheric runs, and three runs with

the manual chopper closed. The bias voltage for all these runs was consistently 26V.

The absolute returns (Figure 38) again show the same pattern as the previous ones, namely a two peaked curve bearing a resemblance to the dark curve for 30 V bias. The problem with stability of the laser output power is apparent from the noisy absolute return curves.

The average D/C and A/C curves (Figures 39 and 40) again show the detrimental effect of the rotating chopper at the lower frequency peak, although here the runs with the manual chopper open show the larger values; the opposite was true in the early November runs. This is a puzzling feature since there were no attempts made to realign the manual chapper. This unexpected behavior is only apparent in the D/C results (Figures 39 and 41) since the A/C differences (Figure 40) are of the same magnitude as the noise (Figure 42). Also for the higher frequency peak an unexpected feature is that the "manual chopper closed" curve is larger at about 74MHz for both the A/C and D/C curve; this effect was partly caused by the averaging process, since one of the chopper runs showing a very low return was interrupted at 72 MHz. The values for both A/C and D/C ratios with the manual chopper open are largest around 70 MHz, which yield a positive peak in the ratio in Figures 41 and 42. The large discrepancies between the A/C and D/C curves further substantiated that problems during this run make the data less reliable than for earlier runs.

5.2 CONCLUSIONS

There is a large influence on the absolute return signal by the non-linear response of the detection system. This is evident not only

in the shapes of the response curves, in general, but also for individual settings of the bias voltage. It was therefore necessary to minimize the influence of this non-linear response in order to retrieve the superimposed actual return signal. This was done by calculating differences and ratios between the return signal with the light chopped and with the light entering the atmosphere. It is felt that this treatment of the data, though not completely eliminating non linear response of the detection system, does suppress these sufficiently to allow an interpretation of the ratios and differences as being indicative of the scattered light. This conclusion is substantiated by the fact that in relatively few runs did maxima or minima in the differences or ratios actually coincide with corresponding features in the absolute returns. There are also runs without a marked peak in the absolute return but still having a large peak in the difference and ratio curves (see e.g., the early November runs). Another substantiating factor is that two observed features occurred consistently in almost all of the more than thirty runs, apparently independently of different bias voltages, data recording and treatment procedures, and chopper configurations. These two signals occur around 62 MHz and 69-72 MHz.

The 69-72 MHz signal always shows up as a peak when the laser light enters the atmosphere and is independent of the chopper configuration. This feature is interpreted as resulting from spontaneous M-B scattering of the laser light. The position of this peak occurs approximately where it can be expected for a CO_2 laser light source. By using the sound velocity as determined ultrasonically by Greenspan[11], we find P(20) and R(20) transitions yield frequencies of 68 and 70.5 MHz.

Our results are in better agreement with Greenspan's[11] sound velocities than those found by Graytak and Benedek[12]. The position of this peak seems to occur either at 69 MHz or at 72 MHz, an interval that would roughly correspond to a change in oscillation from a P transition to a R transition. The width of this peak is estimated to be 4 to 5 MHz which corresponds reasonably well with the theoretical value of 6 MHz; it should however be pointed out that it is difficult to estimate this width since the zero return level is well hidden in the large noise.

The 61 MHz signal is tentatively interpreted as resulting from stimulated M-B scattering. This feature does not coincide with a maximum in the total return as would be expected if it had an instrumental origin. The fact that its behavior changes drastically when the alignment of the rotating chopper is changed from a 90^{o} angle to the laser light (August runs) to another off axis angle (November runs) makes an electronic explanation for the feature even less likely. Attempts to explain this feature in terms of reflection characteristics of the chopper are questionable since one would neither expect such a sharp peak in the reflection from the chopper, nor would this reflection show the demonstrated angular dependence, since the reflection should be of a diffuse nature from the optically rough chopper surface. The threshold nature of the return as apparent in the August runs also decreases the possibility of an electronic or chopper-reflection explanation. The characteristics of this signal can be explained as resulting from stimulated M-B scattering. The effect of the chopper in the August runs was to reflect the sound wave, which had built up in front of the laser by the beat wave between the scattered light and the incident light. This wave, building up co-linearly to the light, would be reflected into the region of the

most intense light, where it would feed its energy into scattered radiation. When the chopper deliberately was realigned after these runs, it no longer reflected the created sound wave at an angle sufficiently colinear to allow interference with the light waves. With this chopper position the chopper merely removed part of the volume from which stimulated emission originated, resulting in less scattering with the chopper closed and in a peak clearly evident in all the remaining runs. The threshold effect apparent in the August returns could be explained by an improvement inthe critical alignment of the chopper, although this was not deliberately done.

The effect of the manual chopper on the reflected light giving the 61 MHz signal is less obvious and more difficult to explain. In the October runs the chopper enhanced the return and continued to do so for the early November runs, although it is not so obvious in the latter case. However in the late November runs this effect seems to be reversed as judged from the $(D/C)_{m.c.o.}/(D/C)_{m.c.c.}$ curve, while the corresponding A/C curve does not show any significant peak or depression, although the late November data was plagued by experimental difficulties making them less reliable. It is possible that a change in the critical alignment of the chopper did occur, though no attempts to do so were made. This feature does behave as would be expected from previous measurements, i.e., it is centered at a frequency lower than that of the spontaneous M-B scattering and has a somewhat narrower halfwidth, on the order of 3-4 MHz.

Although the feasibility of atmospheric remote sensing by M-B scattering has not been demonstrated, nevertheless, characteristics of this type of scattering under atmospheric conditions were apparent in the return signal. These results should encourage further efforts to improve the return signal and correlate its features with atmospheric parameters.

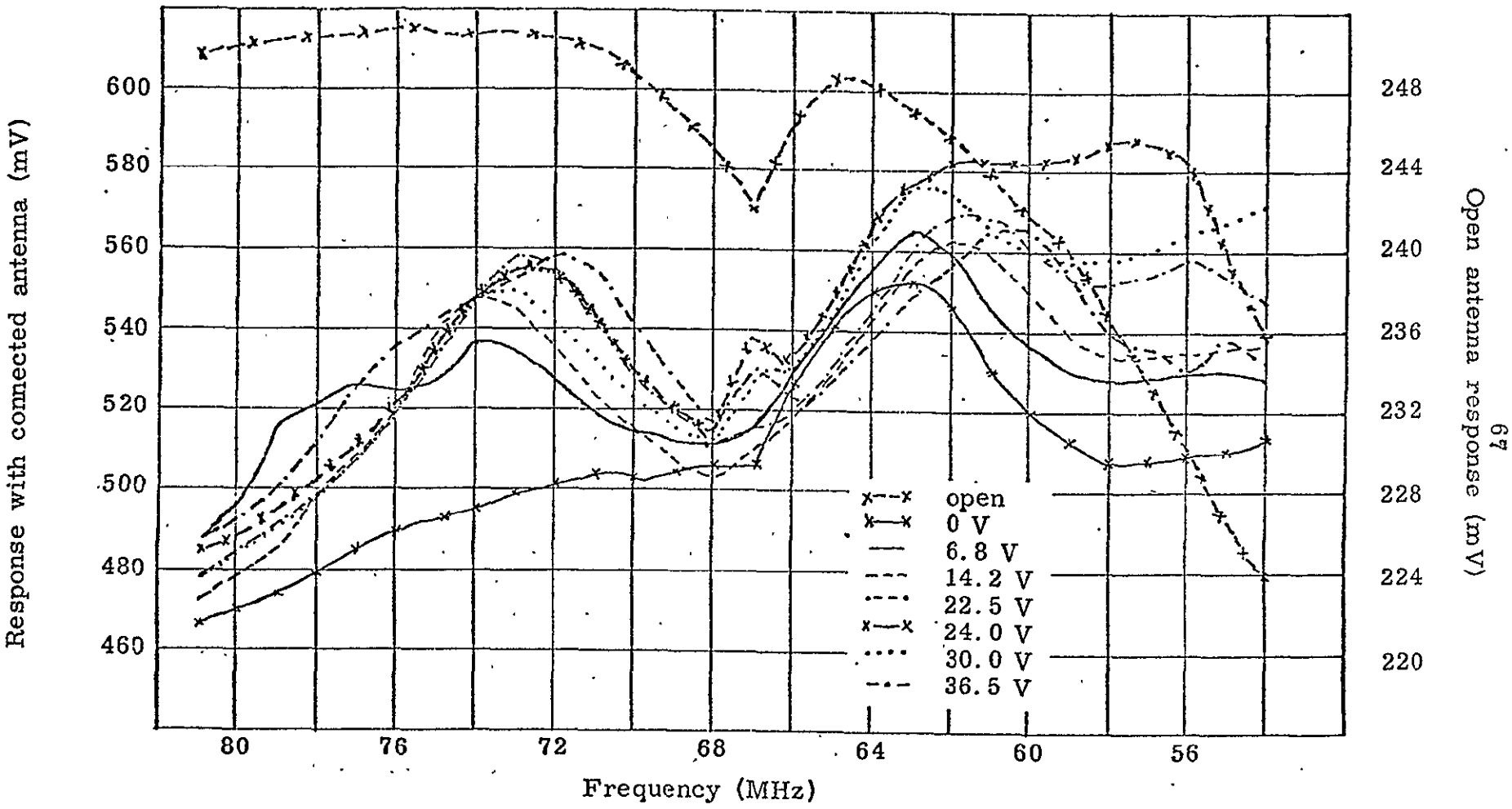

Fig. 25 .- Dark response of receiving system for varying bias voltages.

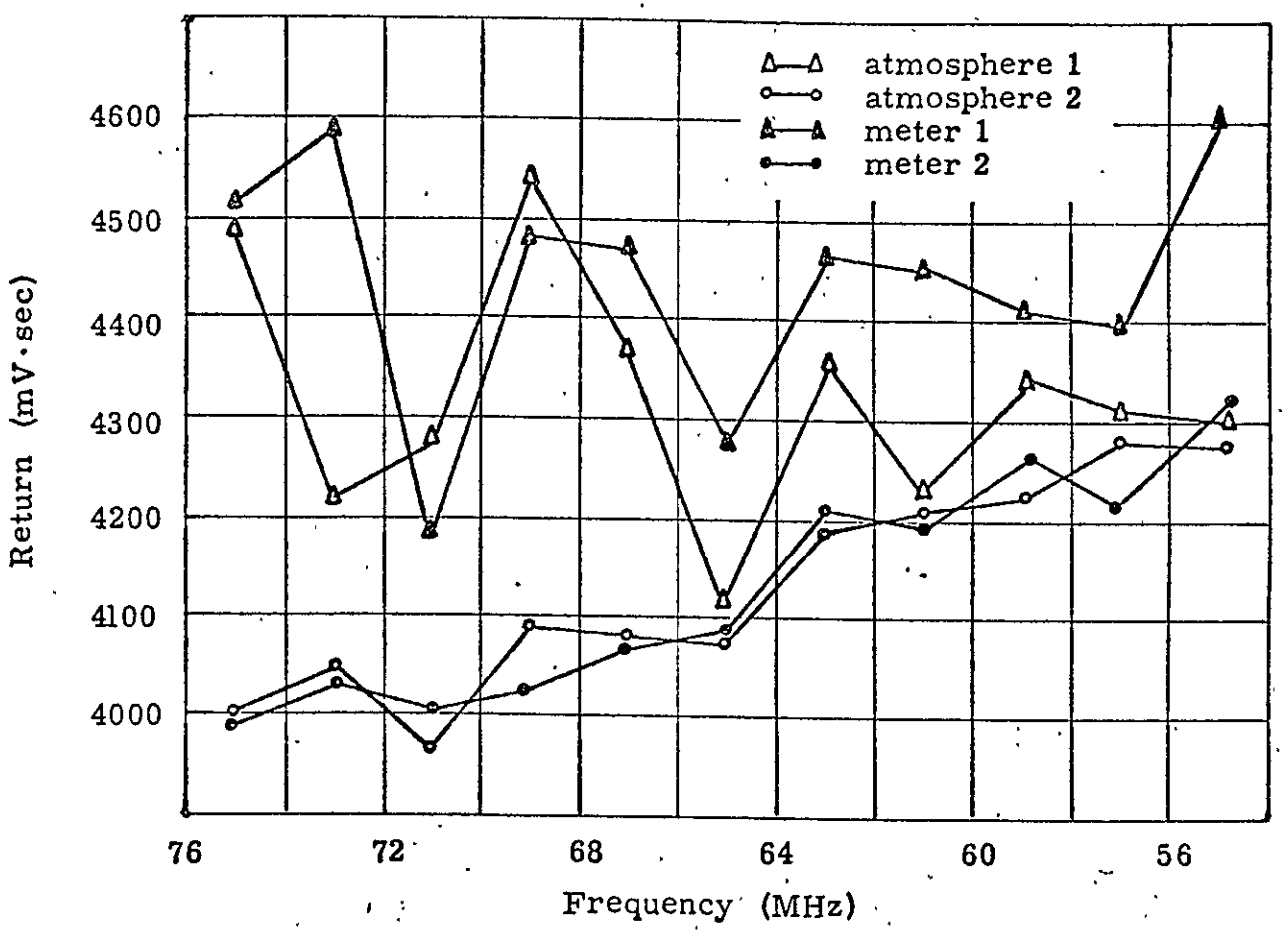

Fig. 26 .- Absolute returns.
Date: July 16, 1970.
Process: Digital integrating voltmeter - power meter.

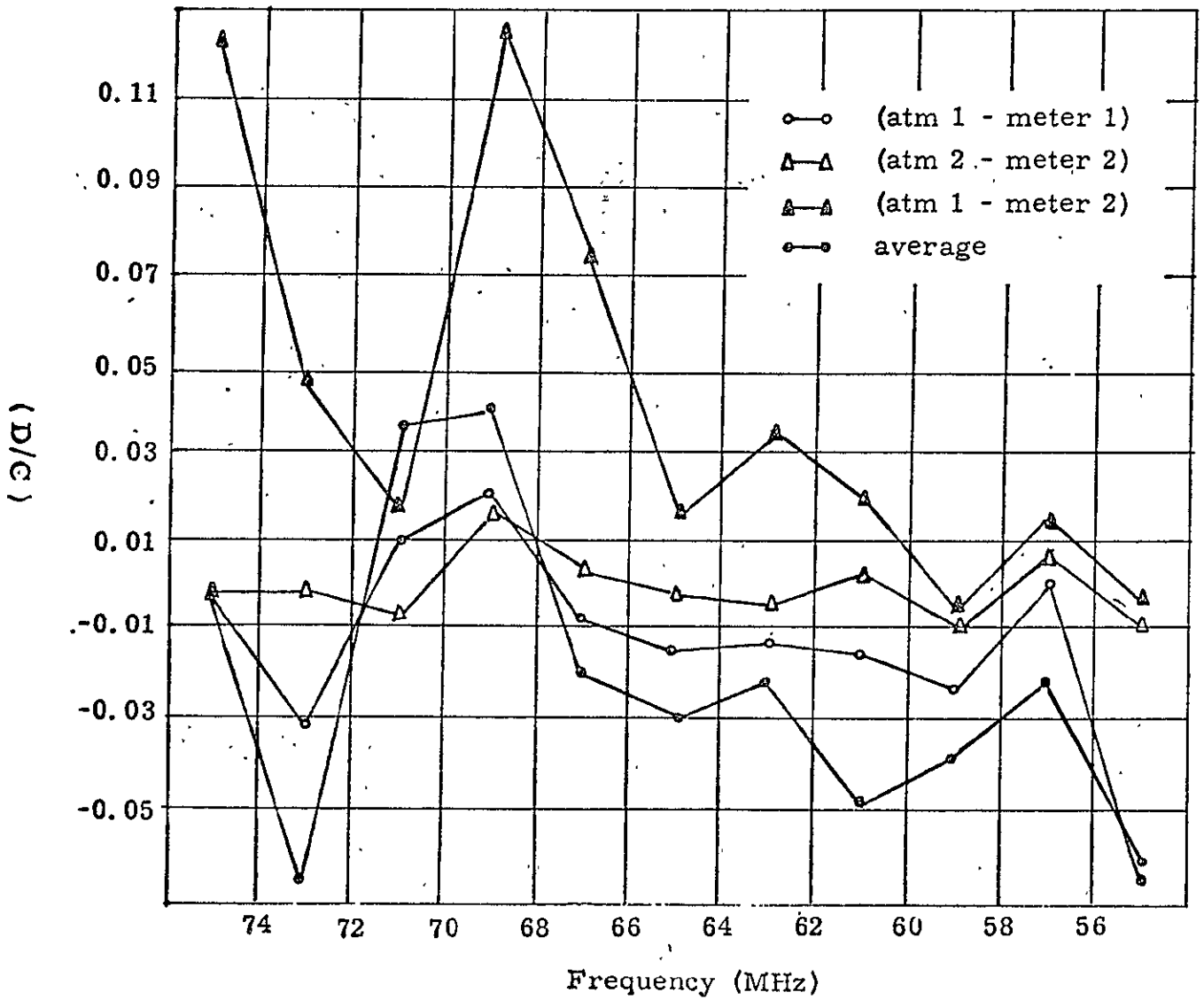

Fig. 27. - (D/C)
Date: July 16, 1970
Process: Digital integrating voltmeter - power meter

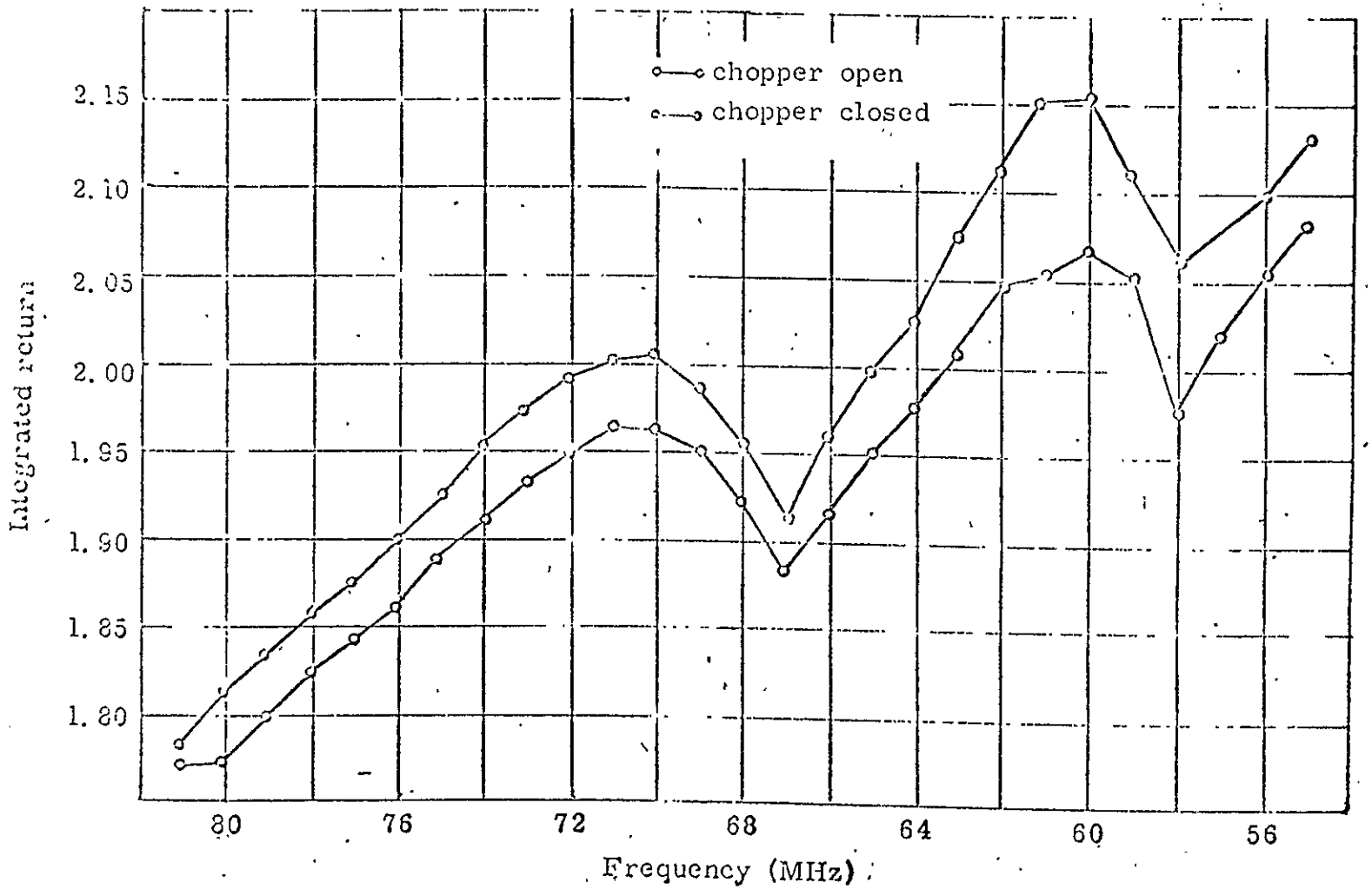

Fig. 28. - Absolute return.
Date: August 22, 1970 - 4th run.
Process: Recorder, computer - rotating chopper.

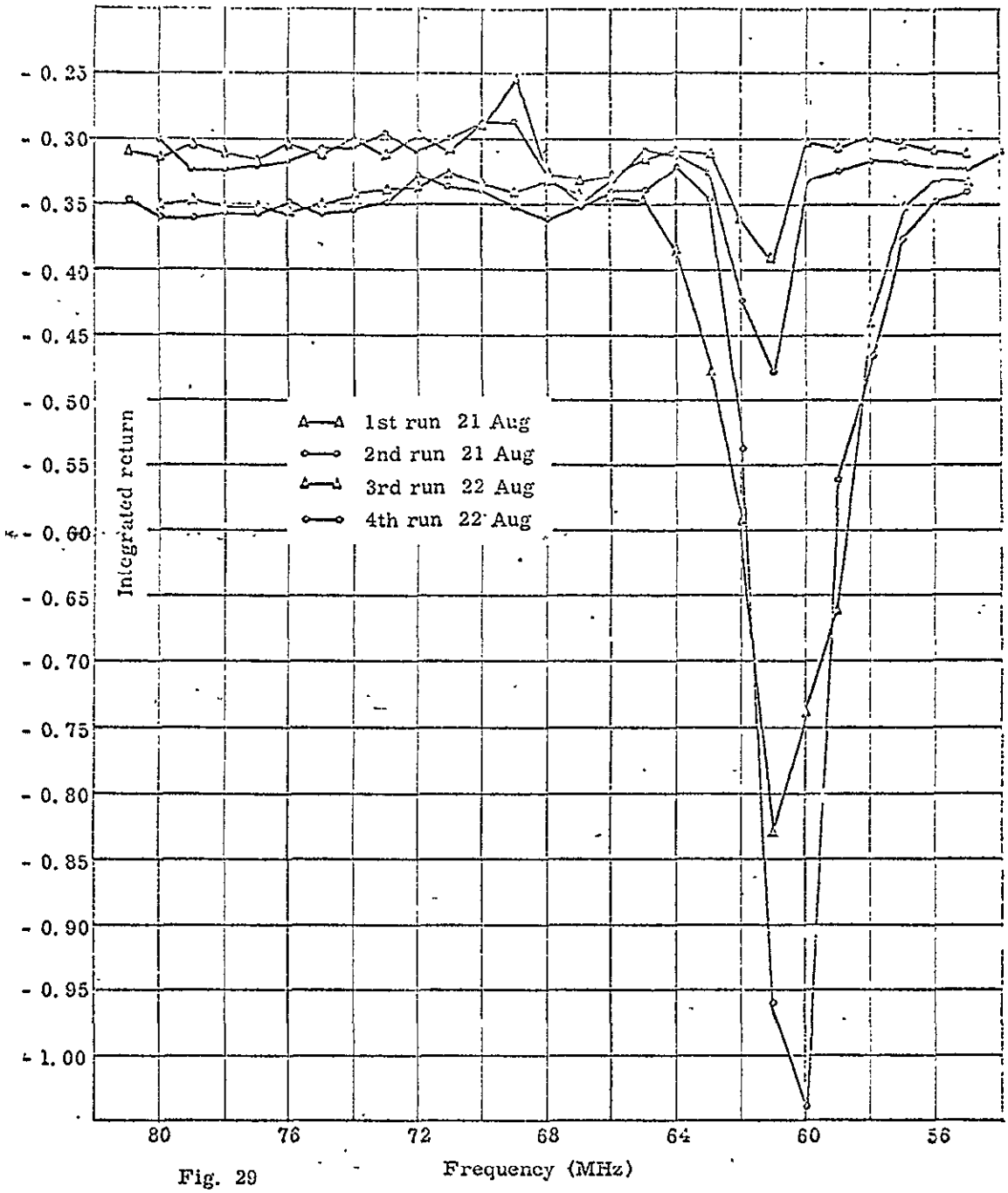

Fig. 29

Individual (D/C)

. Date: August 21 and 23, 1970.

Process: Recorder, computer - rotating chopper.

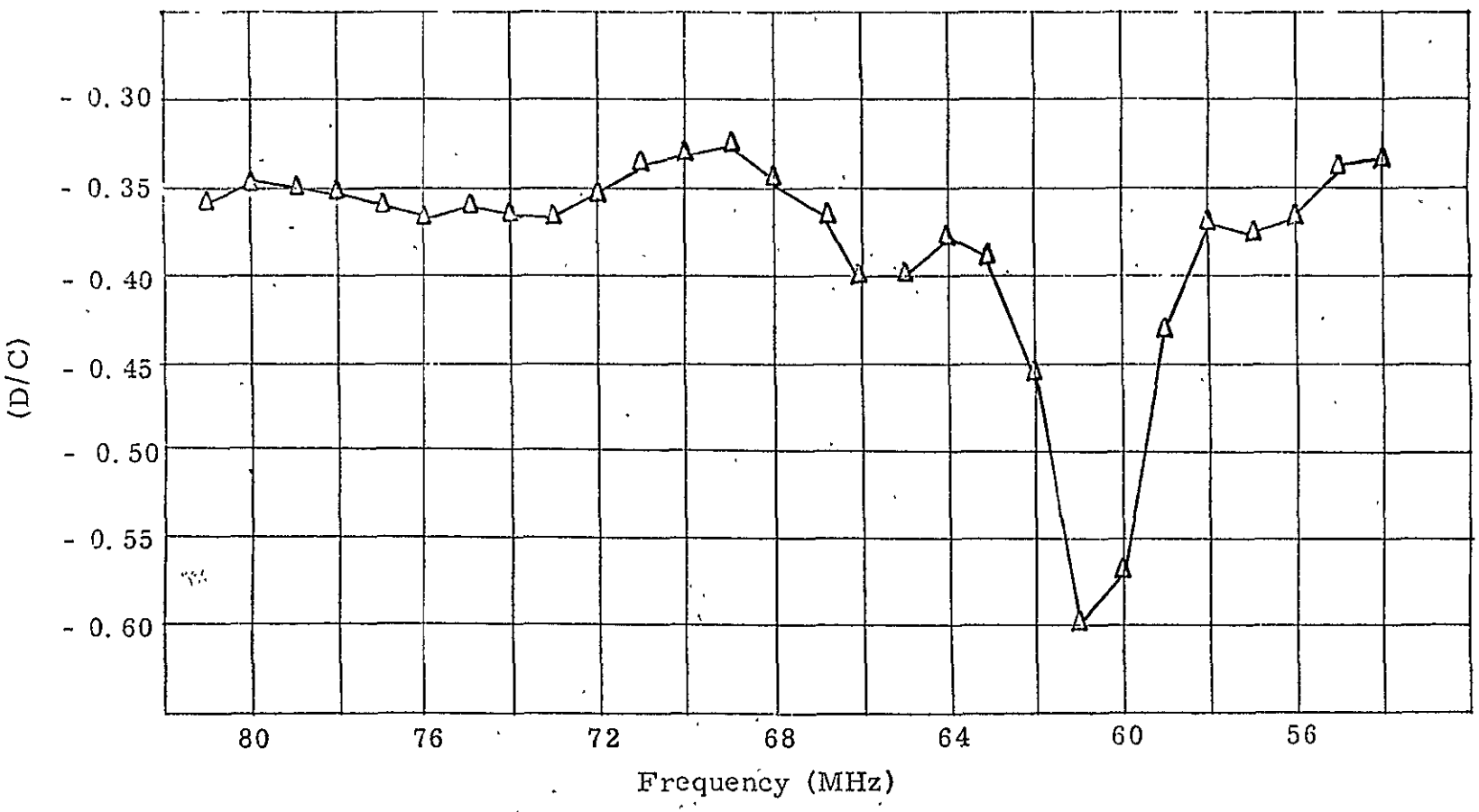

Fig. 30 . - (D/C)

Date: August 18, 21 and 22, 1970.

Process: Recorder, computer - rotating chopper.

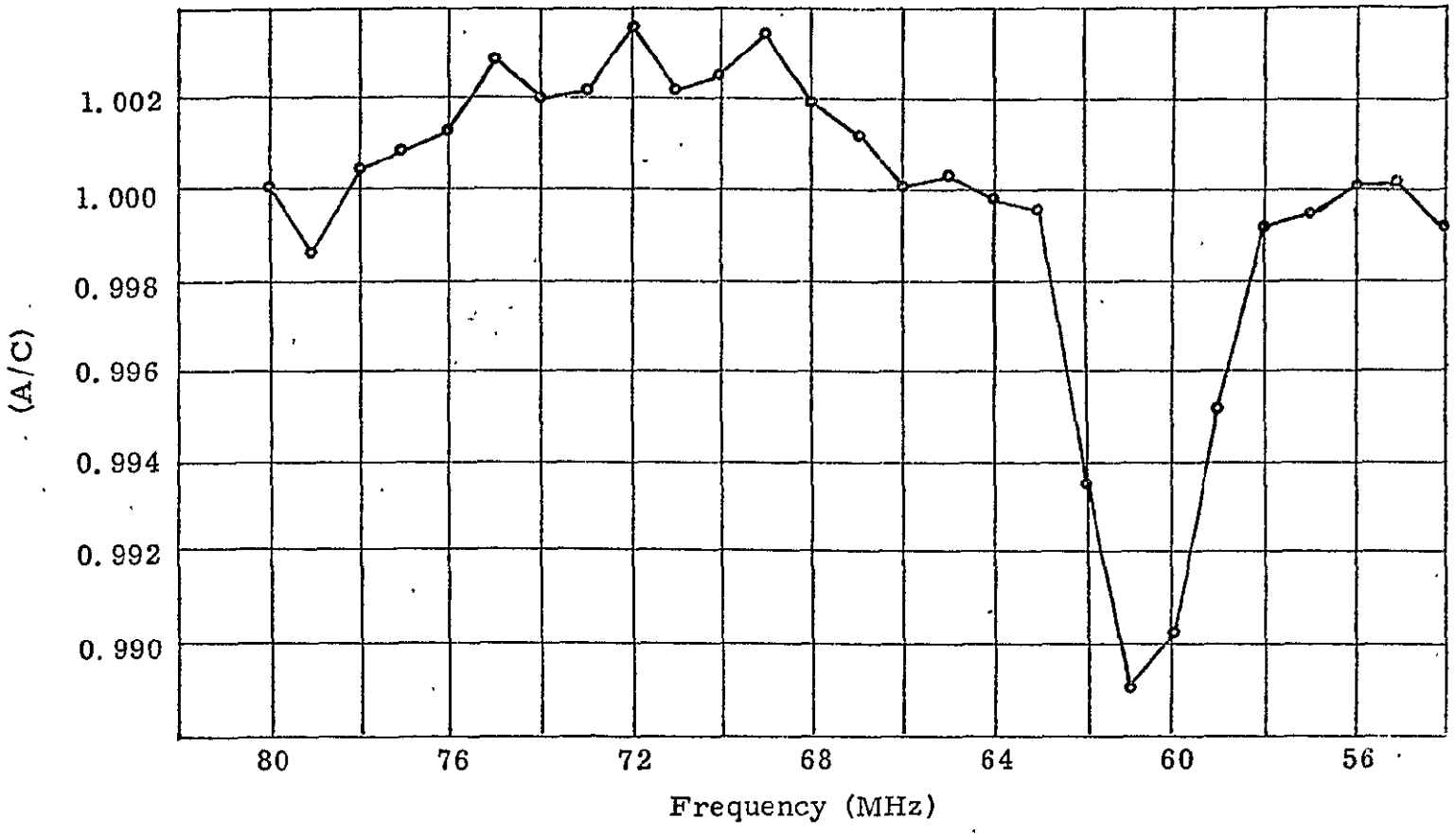

Fig.31 .- (A/C)

Date: August 18, 21 and 22, 1970.

Process: Recorder, computer - rotating chopper.

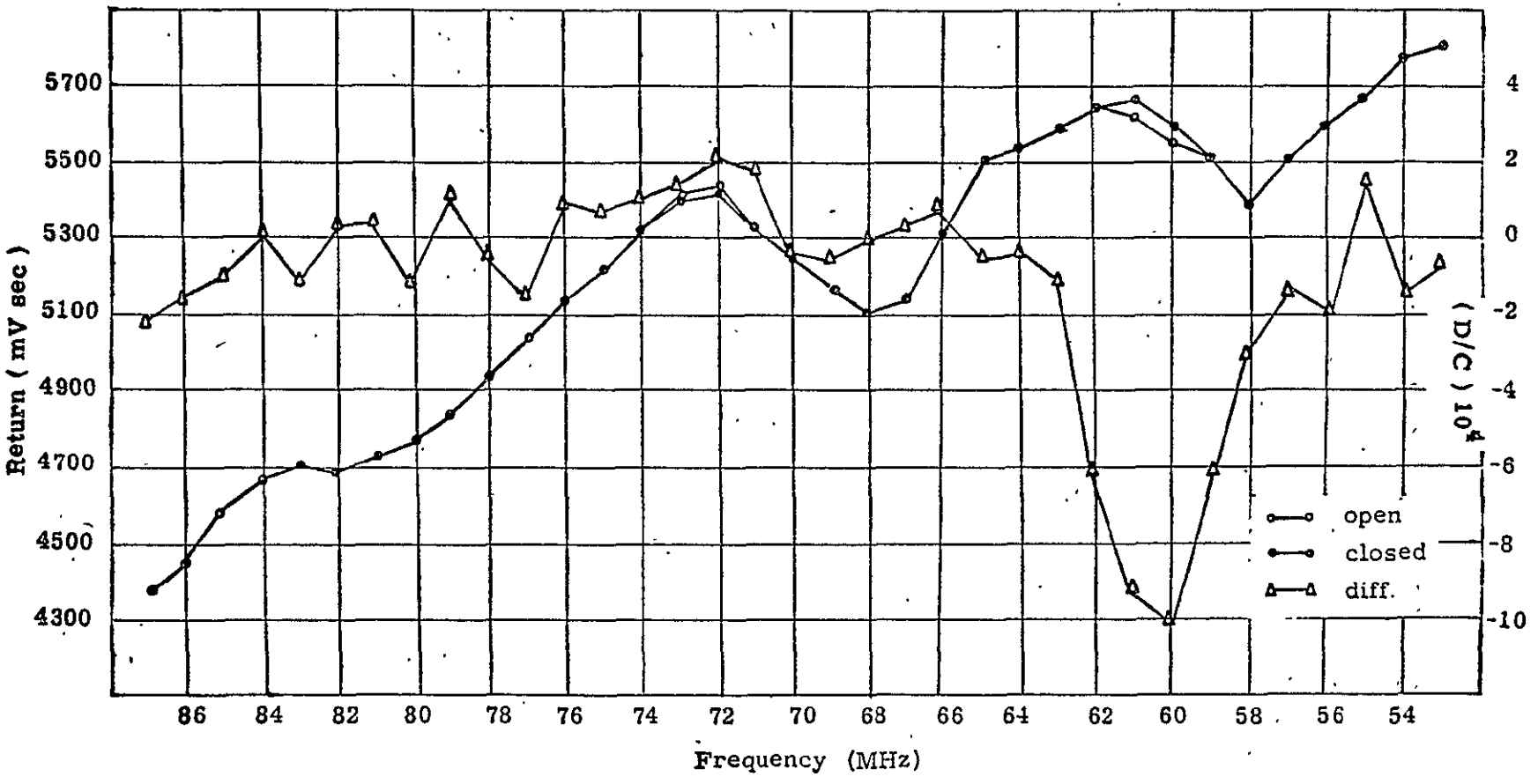

Fig. 32.- Absolute returns and (D/C)

Date: October 18, 19 and 20, 1970

Process: Digital integrating voltmeter - manual chopper.

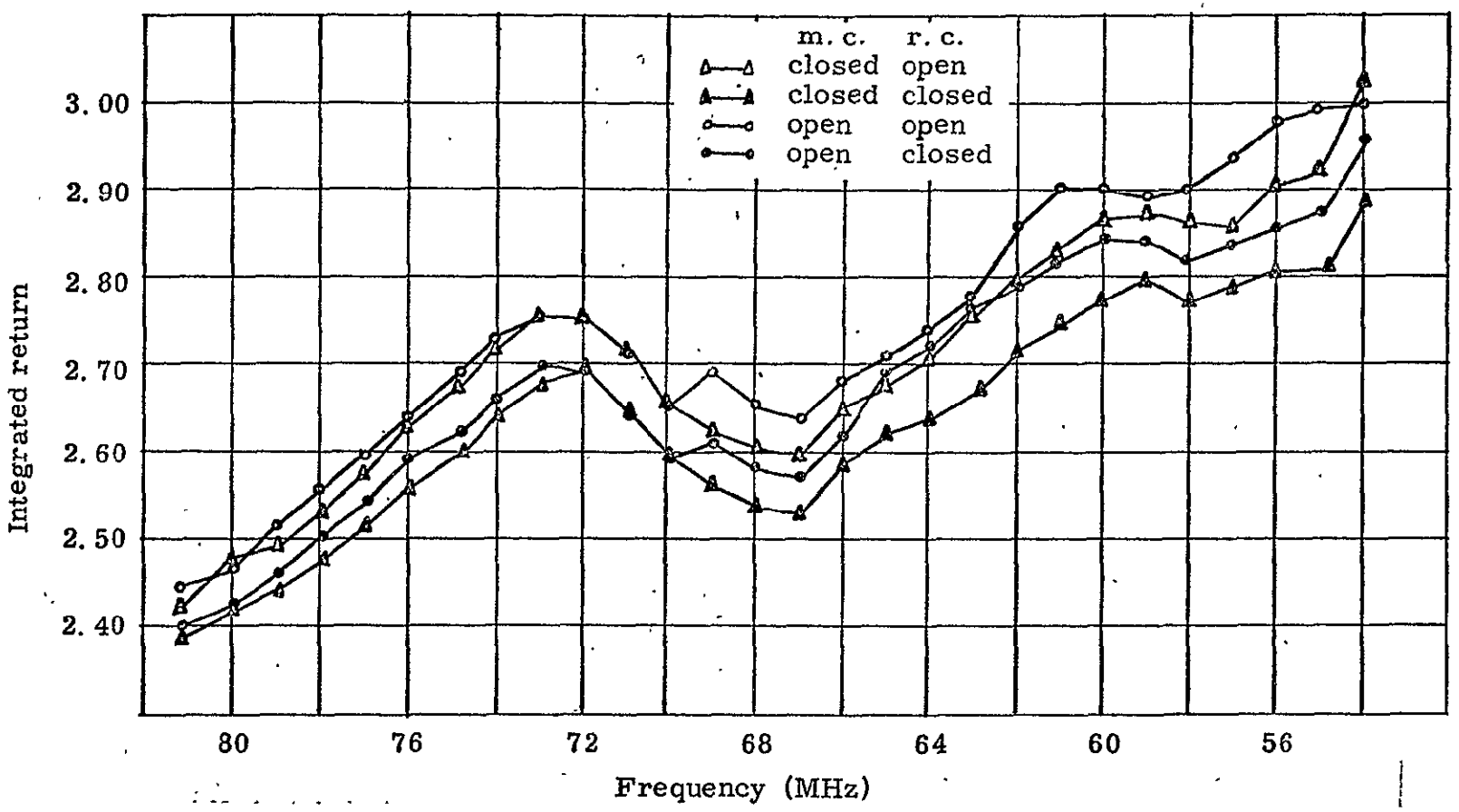

Fig. 33 .- Absolute returns.

Date: November 3 and 5, 1970.

Process: Recorder, computer - rotating and manual choppers.

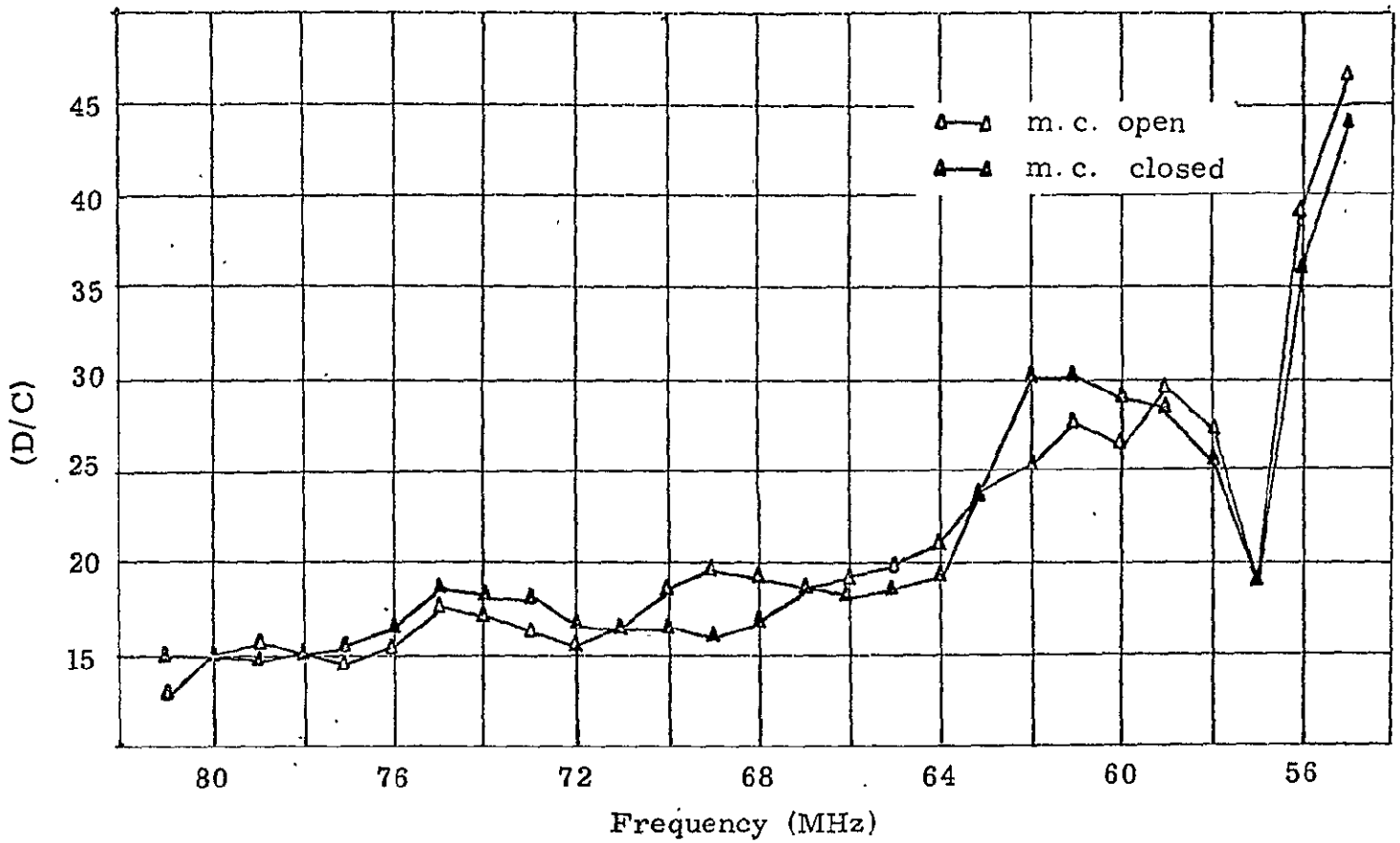

Fig. 34 .- $(D/C)_{\text{manual chopper open}}$ and $(D/C)_{\text{manual chopper closed}}$.
Date: November 3 and 5, 1970.
Process: Recorder, computer - rotating and manual choppers.

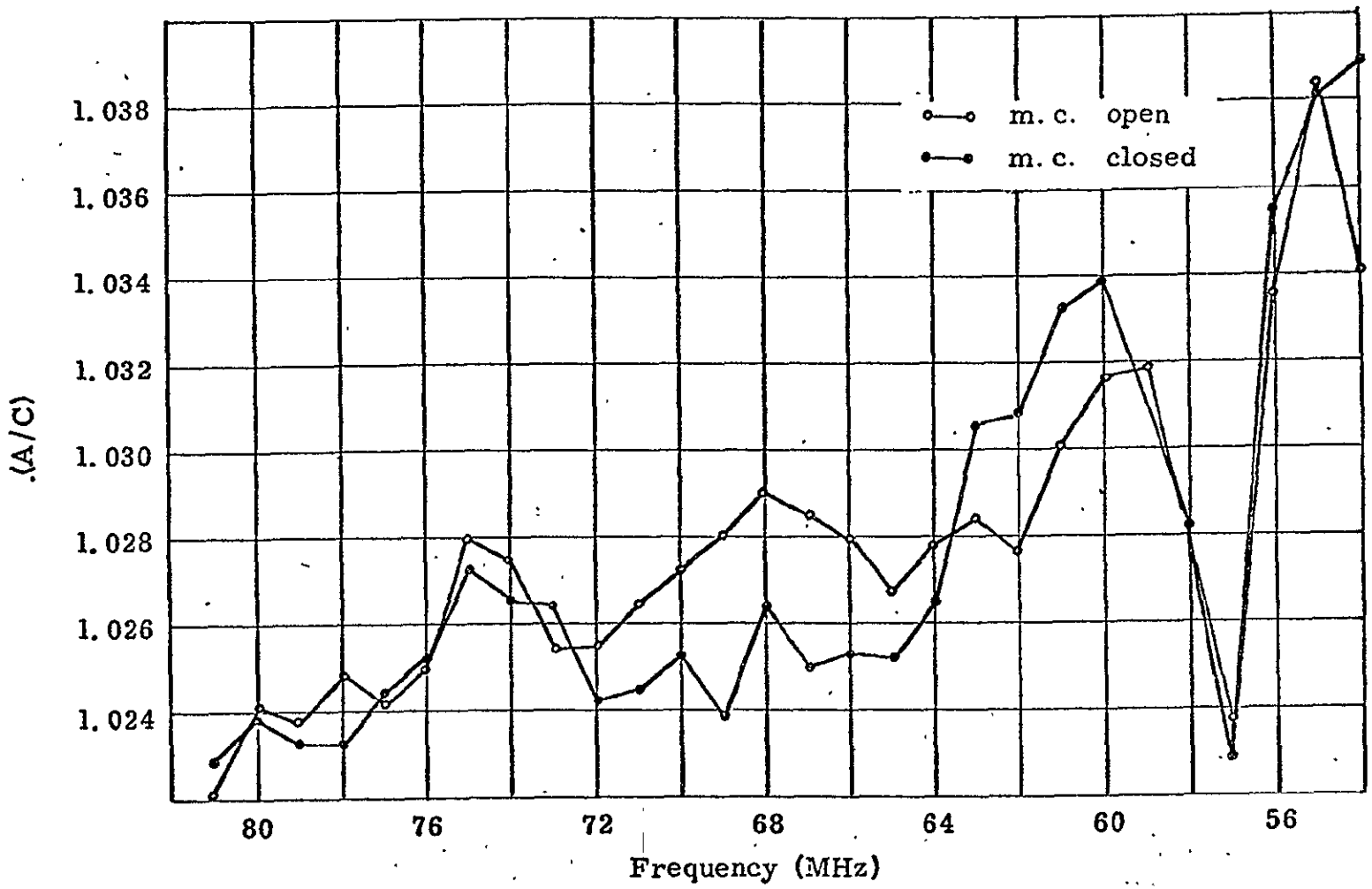

Fig. 35 . - $(A/C)_{\text{manual chopper open}}$ and $(A/C)_{\text{manual chopper closed}}$.
Date: November 3 and 5, 1970.
Process: Recorder, computer - rotating and manual choppers.

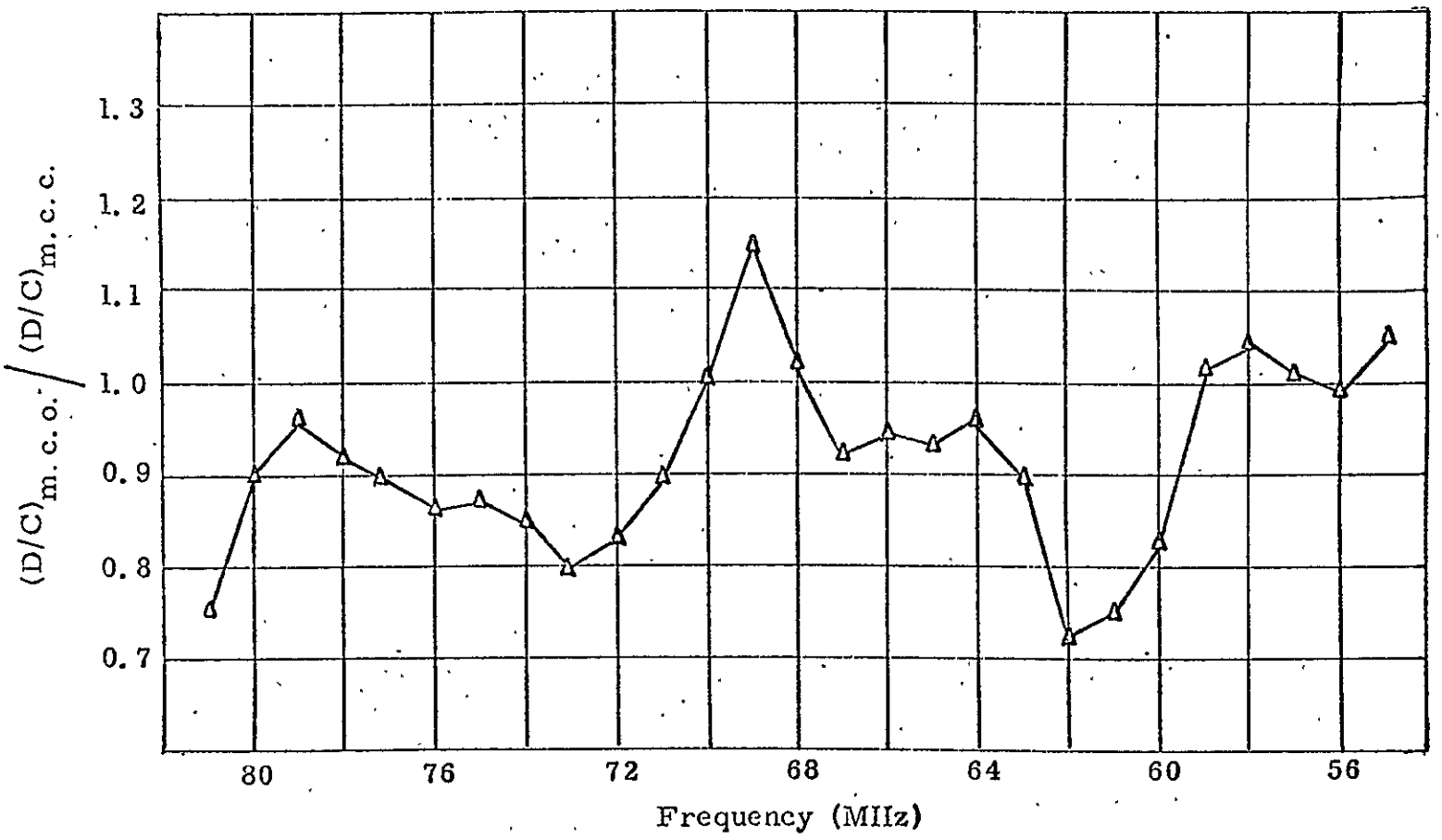

Fig. 36 . - $(D/C)_{\text{manual chopper open}} / (D/C)_{\text{manual chopper closed.}}$

Date: November 3 and 5, 1970.

Process: Recorder, computer - rotating and manual choppers.

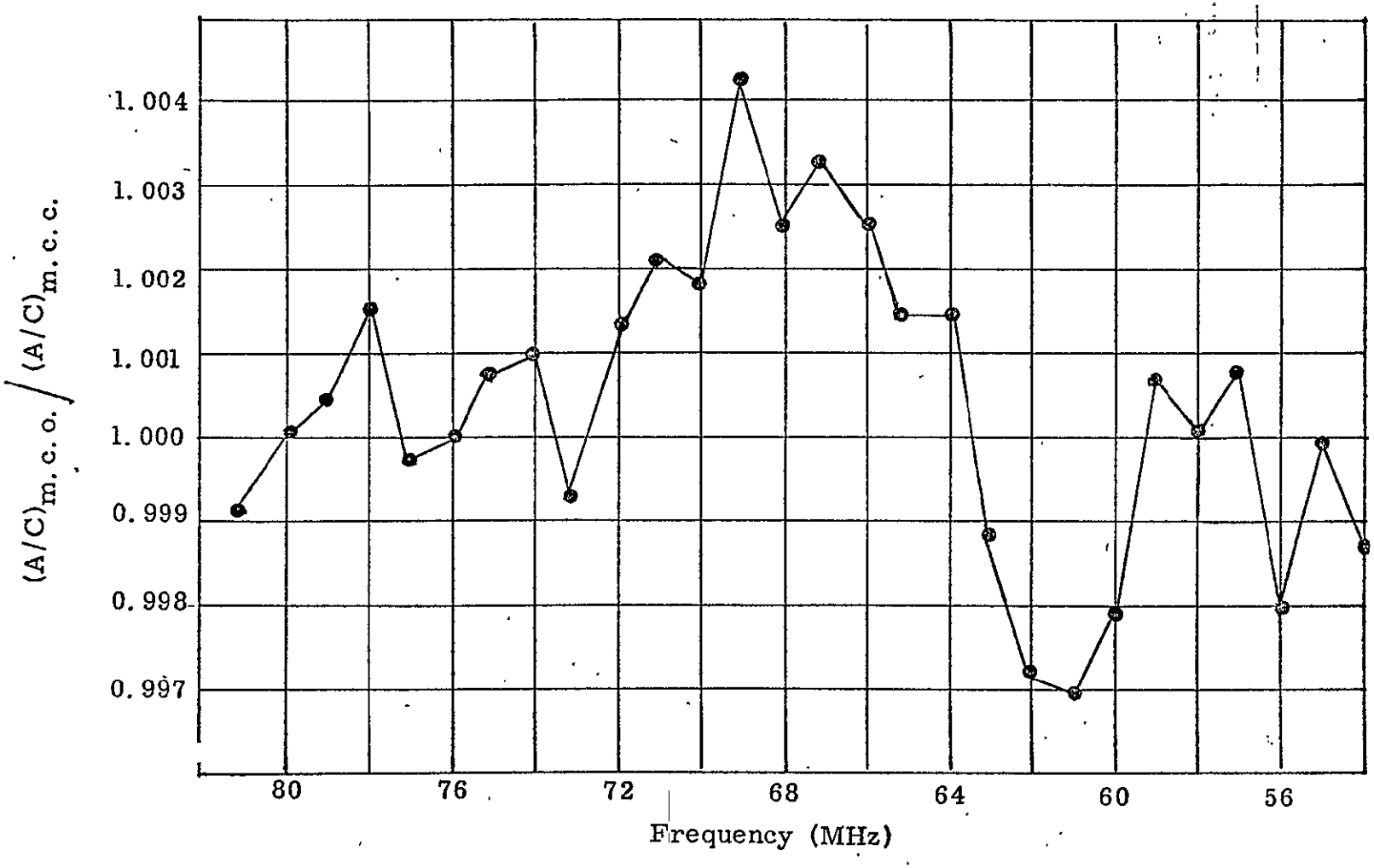

Fig. 37 .- $(A/C)_{\text{manual chopper open}} / (A/C)_{\text{manual chopper closed}}$.
Date: November 3 and 5, 1970.
Process: Recorder, computer - rotating and manual choppers.

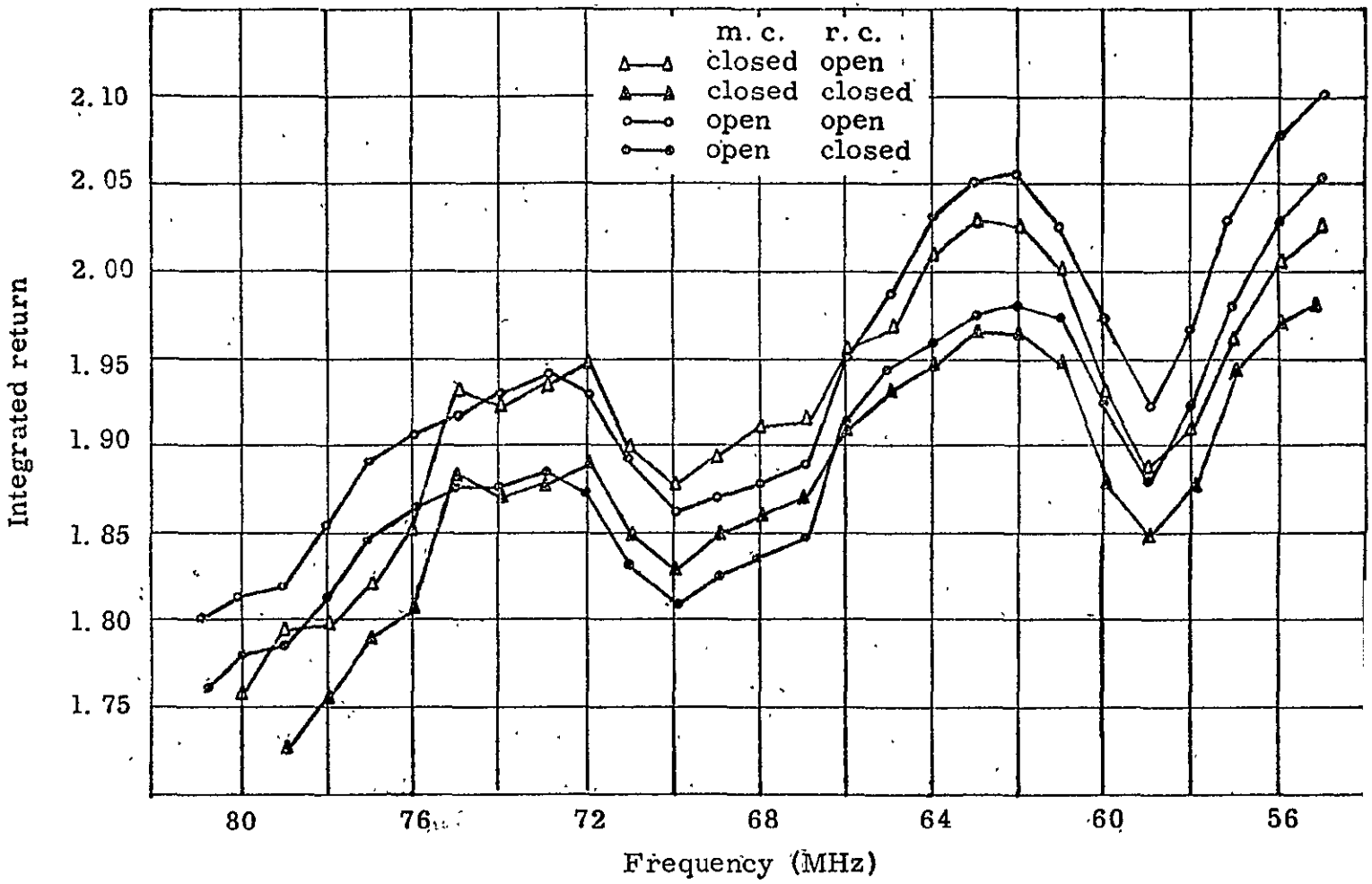

Fig. 38 .- Absolute returns.
Date: November 27 and 30, 1970.
Process: Recorder, computer - rotating and manual choppers.

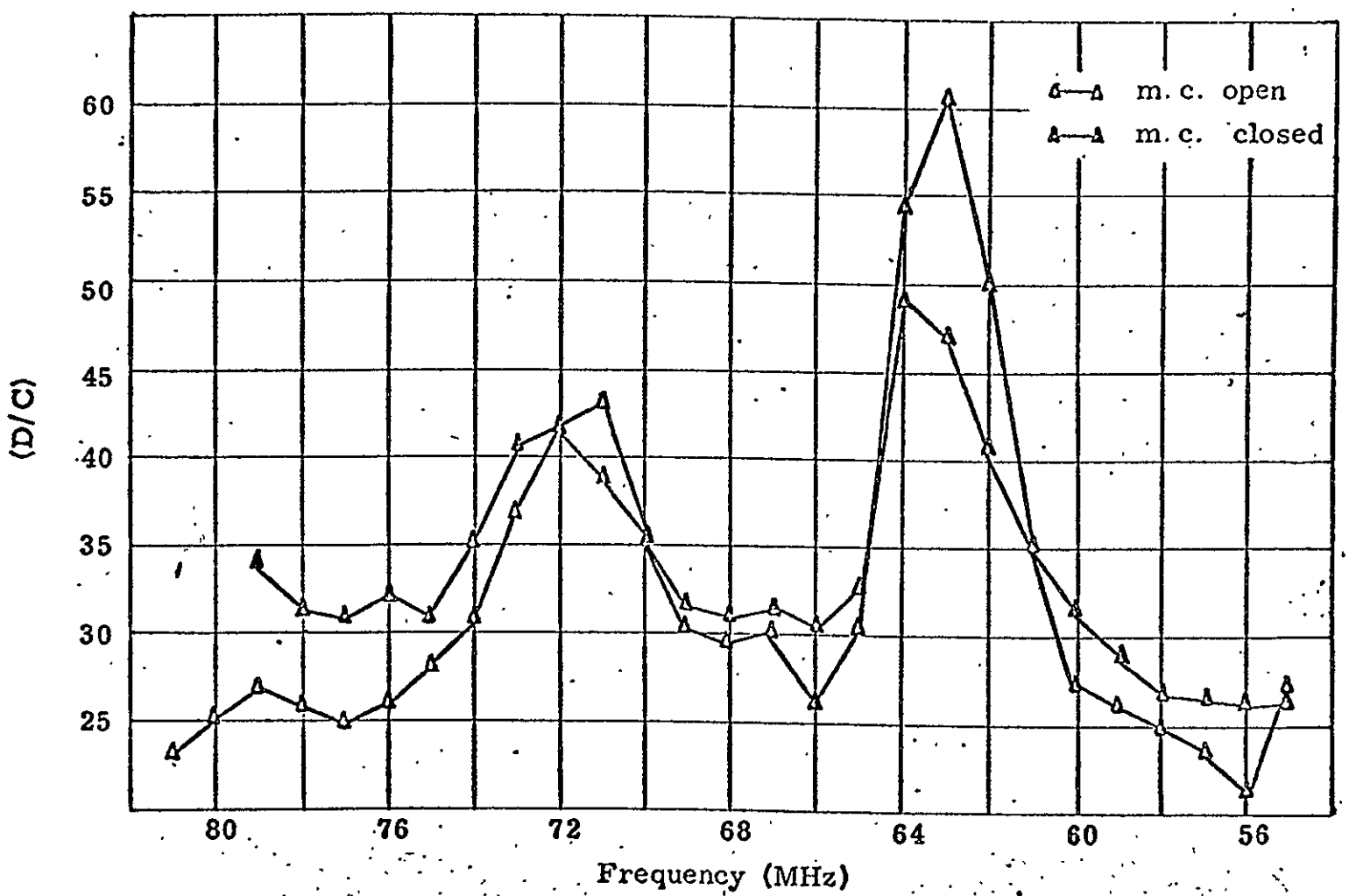

Fig. 39 - $(D/C)_{\text{manual chopper open}}$ and $(D/C)_{\text{manual chopper closed}}$.

Date: November 27 and 30, 1970.

Process: Recorder, computer - rotating and manual choppers.

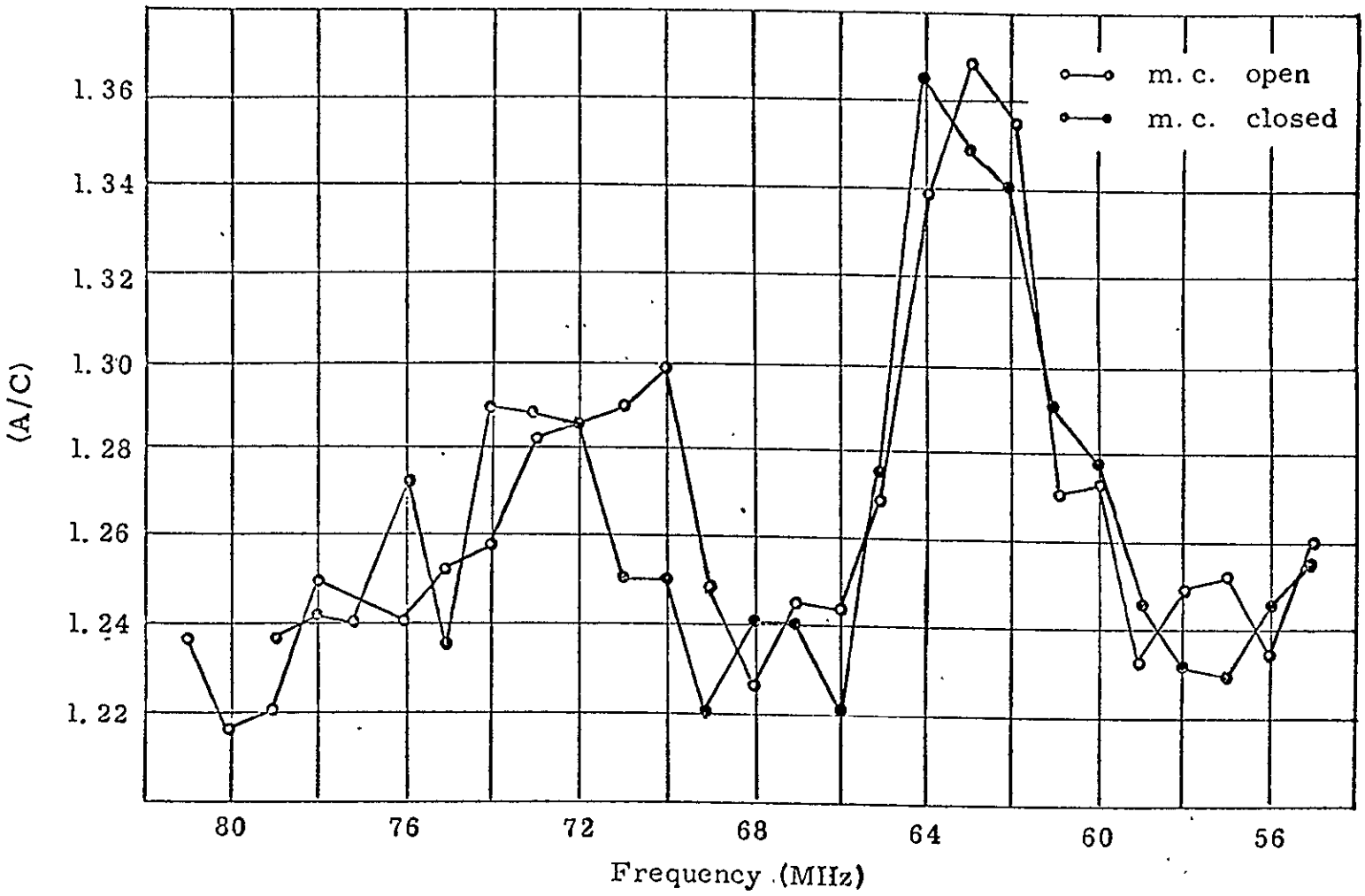

Fig. 40 . - $(A/C)_{\text{manual chopper open}}$ and $(A/C)_{\text{manual chopper closed}}$.
Date: November 27 and 30, 1970.
Process: Recorder, computer - rotating and manual choppers.

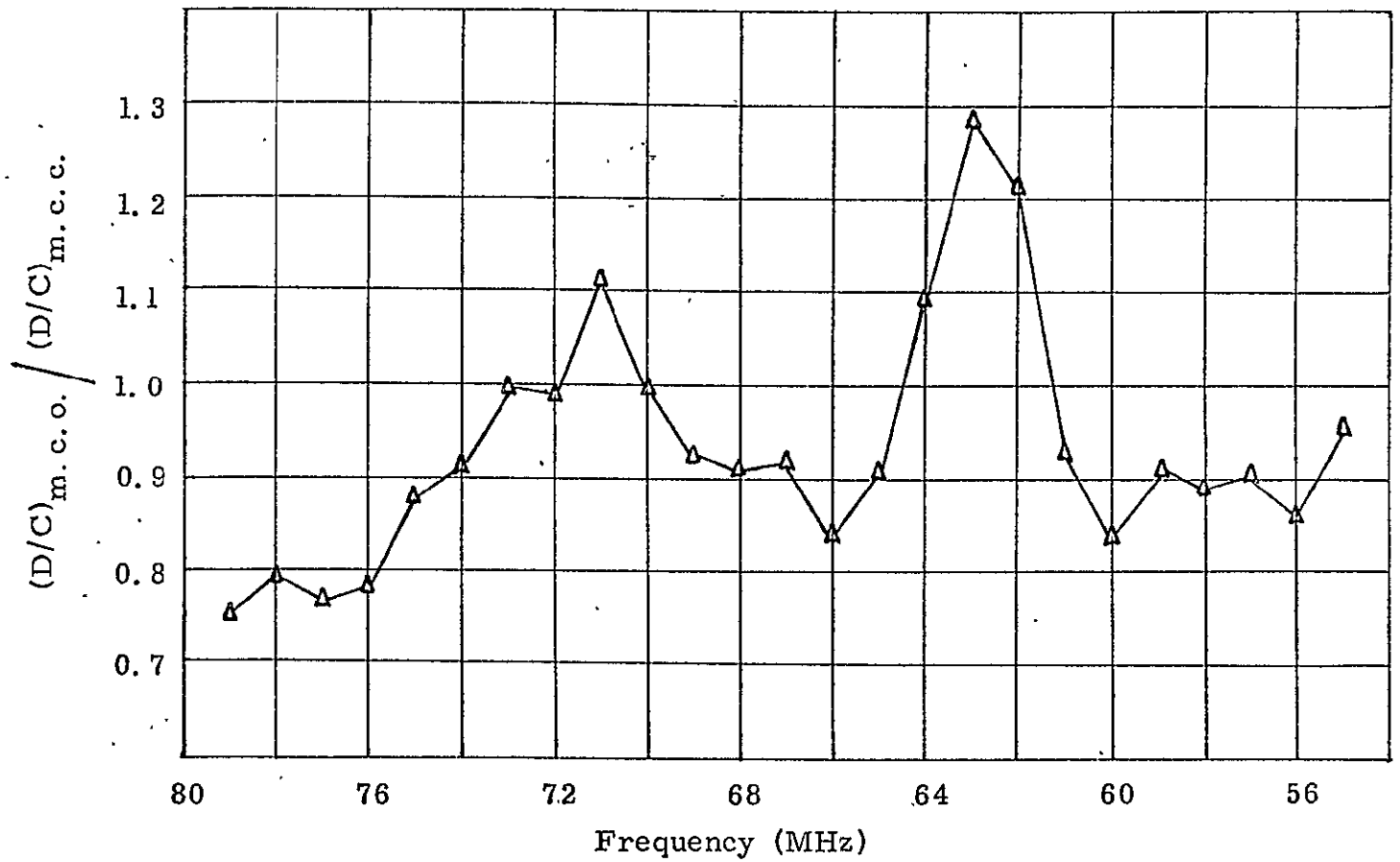

Fig. 41.- $(D/C)_{\text{manual chopper open}} / (D/C)_{\text{manual chopper closed}}$.
Date: November 27 and 30, 1970.
Process: Recorder, computer - rotating and manual choppers.

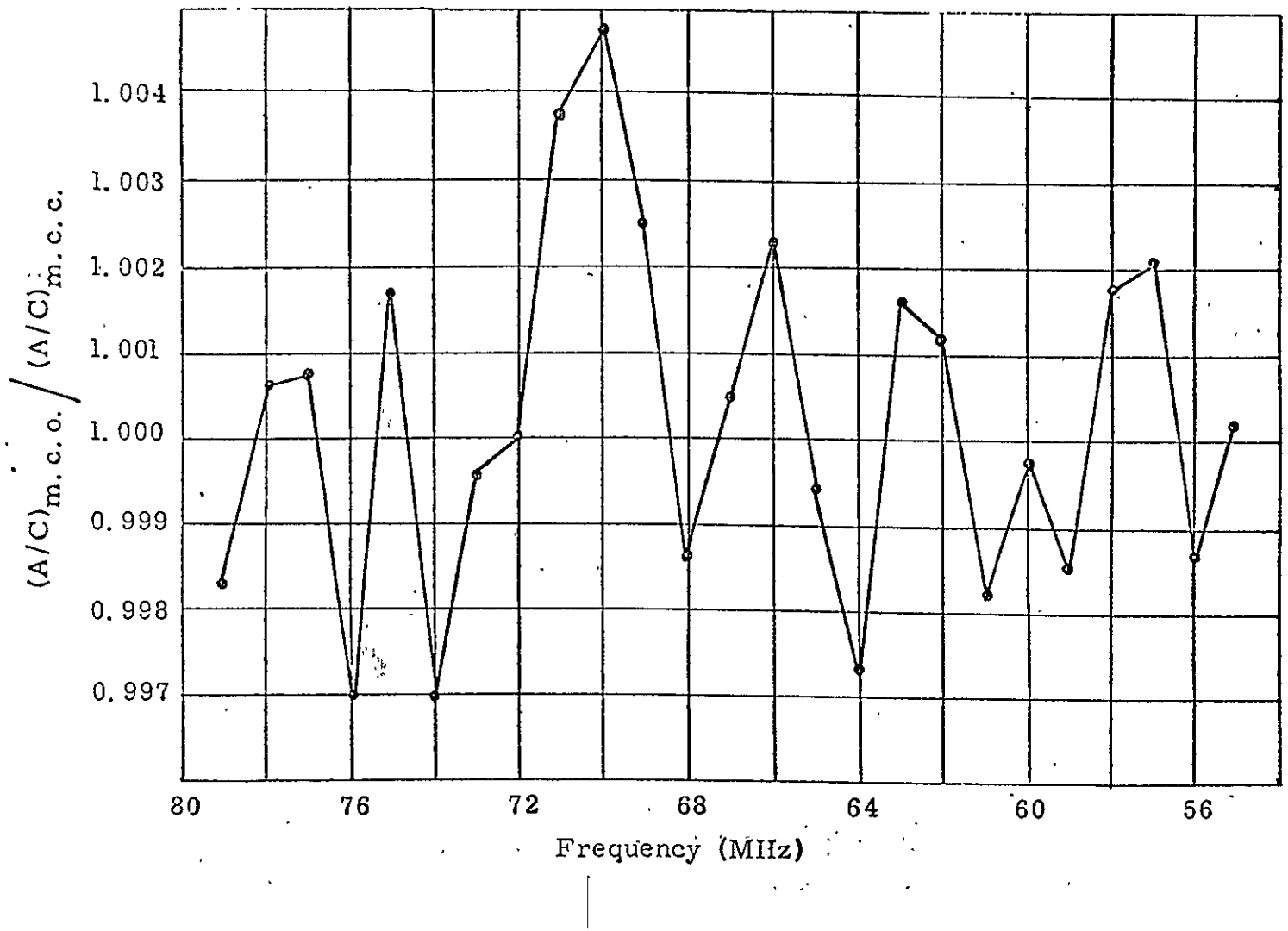

Fig. 42 - $(A/C)_{\text{manual chopper open}} / (A/C)_{\text{manual chopper closed}}$.
Date: November 27 and 30, 1970.
Process: Recorder, computer - rotating and manual choppers.

5.3 SUGGESTIONS FOR FURTHER WORK

Two rather simple but very affirmative tests could be made with the present laser, namely, monitoring the frequency of the laser light and chopper alignment. A spectrometer could be used to monitor the frequency of the laser light. By changing this frequency by moving the differential screw and monitoring the return one should see a change in the frequency of the upper peak in the return, which should correspond to the change in frequency in the emitted light. By mounting the rotating chopper on a rotating table, e.g. a milling head, the alignment of the chopper could be accurately monitored and the effects on the 61MHz feature determined. The above tests could not be made in the present study because of budgetary and time difficulties.

It might be possible to improve the linearity of the detection system by small alterations such as changing the length of the transmission cables or varying the spatial position of some of the components in the detection system. It is however felt that a more substantial improvement would have to include the use of another receiver with more linear response and preferably a lower frequency range.

The experiments would be greatly facilitated if a nitrogen cooled detector with the required high frequency response were available. A test of the frequency response of the detection system to laser light of a constant amplitude would be very valuable, but would require the use of a laser light modulator.

A number of features in the present laser system design could be improved, of which the most urgent is an active stabilization system for the laser output. To improve the S/N ratio for the experiment, the only

parameter that could be changed is the power of the emitted light. Such an improvement would be necessary if spatial resolution were required. A laser with much higher power output is not unrealistic since there exist CO_2 lasers with power outputs 100 times larger than that of the present system.

It is felt that the approach to remote atmospheric sensing using Mandel'stham-Brillouin scattering - both spontaneous and stimulated - should be developed further. No other apparent remote sensing scheme will at present yield both atmospheric temperatures and densities independently of the total return.

APPENDIX

DATA RECORDING AND PROCESSING FOR THE RECORDER COMPUTER-ROTATING CHOPPER COMBINATIONS

The data were recorded on an Ampex tape recorder running at 30 ips. Four channels were used representing the following pieces of information (Figure 20).

a) Chopper position

A lamp and photocell were located directly below the exiting laser beam at the end of the laser amplifier. When the chopper blade was not blocking the laser beam the light from the lamp reached the photocell which responded with a +2.5 volts. When the chopper blocked the laser beam it also blocked the light from the lamp, resulting in a -2.5 volts generated by the photocell. After being squared by an electronic circuit the pulse was recorded, thus supplying information as towhether the laser beam was entering the atmosphere or being blocked. The time period required for the chopper to go from an open position to a closed one was about 70 m sec. This period will be referred to as the chopper period. The chopper signal could be overridden by a one second pulse triggered manually by a microswitch. This pulse was used to indicate a change in the frequency setting of the receiver.

b) Receiver strength

During a data run the frequency setting of the receiver was changed in 1 MHz steps from 55 MHz (the lower limit of the reciever) to about 80 MHz (end of the tape). The bandwidth of the receiver was 600 KHz. The receiver had a low frequency voltage output proportional to the incoming high frequency signal. This low frequency signal was

amplified and recorded on the second track of the tape recorder. One minute was used on each frequency setting, and this one minute period will be referred to as the frequency period. The beginning of each frequency period was identified by pressing the microswitch which resulted in a long pulse on the chopper track.

c) Laser output power.

Since the returned signal is proportional to the outgoing signal, this quantity was monitored and recorded on the third track of the tape.

d) Bias current

The local oscillator power, which is proportional to the VHF signal was monitored by recording the DC bias current on the fourth track.

DATA PROCESSING

The purpose of the data processing is to recover the small signal from the noise by using time integration. This integration was done by a hybrid computer in two steps. First an analog section integrated the signal over one chopper period and sent the result via an analog to digital converter to the digital section, a PDP-8 computer, which stored the values and averaged them over one frequency period. In this section we will first describe in detail the analog section and secondly, the program for the digital computer.

a) The analog section

The analog section had three major parts: the chopper signal processor, the signal integrator, and the monostable. The chopper signal processor converted the chopper signal into a series of sharp alternating pulses, a negative pulse marking the beginning of a blocked

period, while a positive pulse marked the beginning of an unblocked chopper period. This pulse train informed the digital computer when to read the analog to digital converter to which the receiver signal was sent after integration, and to start the analog integrator. The integrator could be set to integrate on positive chopper only, i. e. integrate the return when the laser beam was not blocked from the atmosphere, integrate on negative chopper only, i. e. integrate when the beam was blocked, or first integrate positively on positive chopper and then to negatively integrate on negative chopper, the net result thus representing the difference in return between two consecutive chopper positions. This procedure was more accurate than to have the digital computer subtract the first two alternatives. To compensate for variations in the chopper period, it was necessary to introduce a monostable, which interrupted the integration after a fixed time interval somewhat less than the chopper period. The time sequence for an integration corresponding to the first and last alternatives is shown in Figure 43.

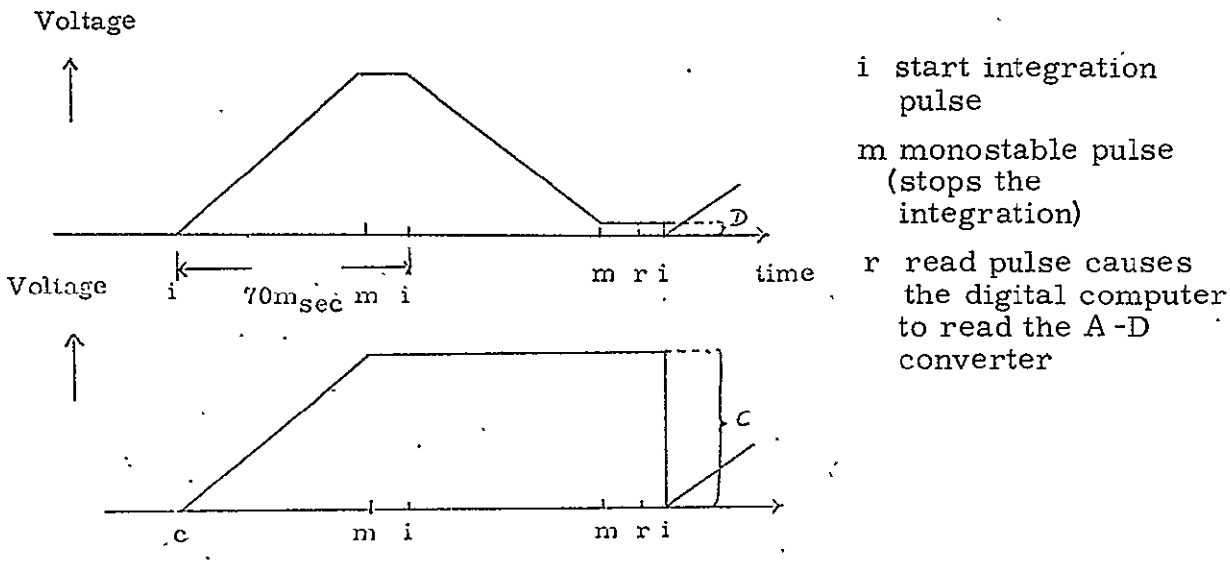

Figure 43. Integration sequence for difference integration (above) and chopper integration (below).

The signal representing the bias current and the laser output power were continuously averaged by a resistor-capacitor circuit having a time constant of 45 seconds. This combination supplied the digital computer with signals already averaged over the frequency period.

DIGITAL PROCESSING

The analog section of the computer provided the digital section with the following four signals:

a) a flag indicating when the computer should read the analog to digital converter to which the integrated signal was sent.

b) a signal proportional to one of the following quantities:

1) the integrated return signal with the chopper open (A)

2) the integrated return with the chopper blocking the beam from the atmosphere (C)

3) the integrated difference between two consecutive chopper bladesand the atmosphere(D)

c) an averaged laser power signal

d) an averaged bias current signal

A change in the frequency setting of the receiver was accompanied by engaging a microswitch which overrode the chopper signal thus producing a longer pulse. This pulse produced a longer integration time of the receiver signal which resulted in an exceptionally large value of the integrated signal. This large signal was used by the digital computer to start averaging for the next frequency period. Though several quantities could be calculated from the output of the digital computer the most valuable ones were judged to be A/C and D/C. The data were treated by the digital computer as shown on the flow diagram below.

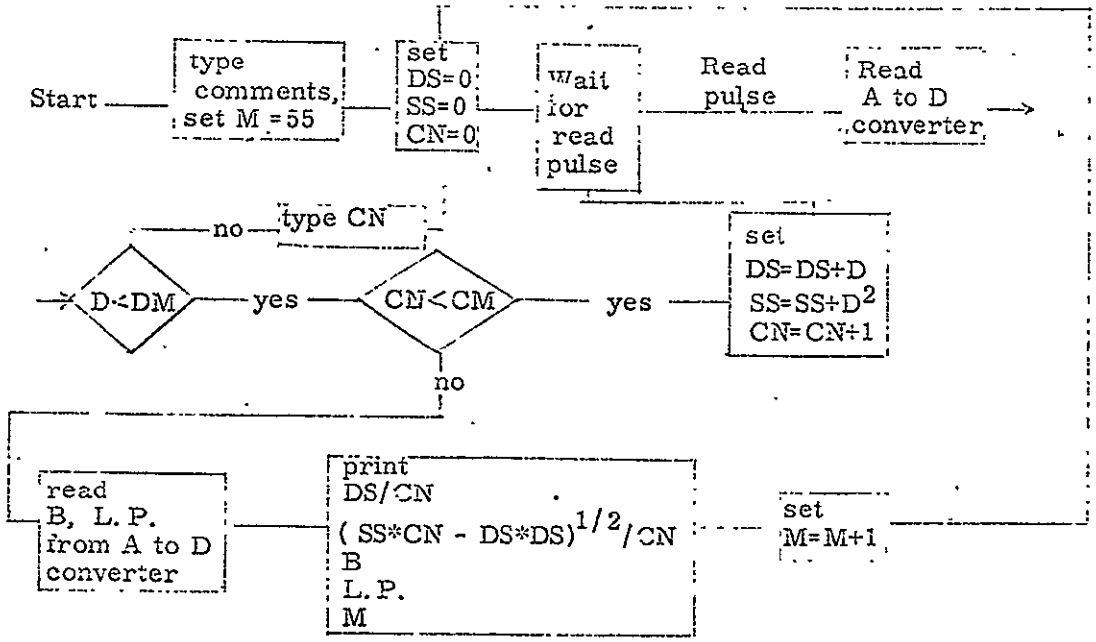

Abbreviations:

M	frequency period counter	D	data from the A to D converter
CN	chopper period counter	D^2	data squared
DS	data summation	SS	data squared summation
L. P.	laser power	B	bias current
CM	max number of chopper periods in one frequency period	DM	max data value

Fig.44 Flow diagram for the digital computer.

BIBLIOGRAPHY

1. J. D. Lawrence, Jr., M. P. McCormic and S. H. Melfi, Optical Radar Studies of the Atmosphere, Presented at the Fifth Symposium on Remote Sensing of Environment, Ann Arbor, Mich., April 16-19, 1968.

2. R. M. Schotland, J. Bradley and A. Nathau, Optical Soundings III, Technical Report ECOM-02207-F, June 1967.

3. E. D. Harris, L. J. Nugent and G. A. Cato, Laser Meteorological Radar Study, Air Force Cambridge Research Laboratories, Bedford, Mass. Report under contract No. AF 19(628)-4309, Jan. 1965.

4. R. M. Schotland, A. M. Nathan, E. A. Charmach, E. E. Uthe and D. Chang, Optical Sounding. Technical Report No. 3, under contract No. DA-36-039 sc 87299. U. S. Army Electronics Research and Development Laboratory, Fort Monmouth, N. J., 1962.

5. I. L. Fabelinskii, Molecular Scattering of Light, (Plenum Press, New York 1968).

6. Lord Rayleigh, Scientific Papers, Vols. I and II (University Press, Cambridge 1899).

7. J. Frenkel, Kinetic Theory of Liquids (Oxford University Press, London 1946).

8. P. Debye, Ann. Physik 39, 789 (1912).

9. L. Landau and G. Placzek, Physik z Soviet Union 5, 172 (1934).

10. R. Penndorf, J. Opt. Soc. Am. 47, 161 (1957).

11. M. Greenspan, J. Acoust. Soc. Am. 31, 155 (1959).

12. I. J. Greytak and G. B. Benedek, Phys. Rev. Letters 17, 4 (1966).

13. T. T. Saito, L. M. Peterson, D. H. Rank and T. A. Wiggins, J. Opt. Soc. Am. 60, 749 (1970).

14. N. Goldblatt, Appl. Optics 8, 1559 (1969).

15. E. E. Hagenlocker and W. G. Rado, Appl. Phys. Letters 7, 236 (1965).

16. D. I. Mash, V. V. Morozov, V. S. Starunov, and I. L. Fabelinskii, JETP Letters (English transl.) 2, 349 (1965).

17. D. H. Rank, T. A. Wiggins, R. V. Wick, D. P. Eastman and E. H. Guenther, J. Opt. Soc. Am. 56, 174 (1966).

18. Atmospheric Explorations by Remote Probes, Vol. 2. Final Report of the Panel on Remote Atmospheric Probing to the Committee on Atmospheric Sciences, National Academy of Sciences, National Research Council, 1969.

19. L. B. Loeb, The Kinetic Theory of Gases (Dover Publications Inc., New York 1961).

20. D. L. Fried, Proc. IEEE 55, 57 (1967).

21. R. T. H. Collis, J. Roy. Meteorol. Soc. 92, 220 (1966).

22. A. E. Siegman, Proc. IEEE 54, 1350 (1966).

23. D. Meyerhofer, IEEE J. Quantum Electron QE-2, 969 (1968).

24. M. C. Tiech, Proc. IEEE 56, 37 (1968).

25. P. K. L. Yin and R. K. Long, Appl. Optics 7, 1551 (1968).

26. W. Y. Ramsey, Specular Spectral Reflectance of Paint from 0.4 to 40 microns, Meteorological Satellite Laboratory Report No. 31, to U. S. Weather Bureau, National Weather Satellite Center, Washington, 1964.

27. C. J. Buczek and G. S. Picus, Appl. Phys. Letters 15, 125 (1967).